2021

Developing persulfate-activator soft solid (PASS) as slow release oxidant to remediate phenol-contaminated groundwater

Maneekarn Yoo-iam
Kasetsart University, Bangkok

Tunlawit Satapanajaru
Kasetsart University, Bangkok, fscitus@ku.ac.th

Chanat Chokejaroenrat
Kasetsart University, Bangkok

Chainarong Sakulthaew
Kasetsart University, Bangkok

Steve Comfort
University of Nebraska-Lincoln, scomfort1@unl.edu

See next page for additional authors

Developing persulfate-activator soft solid (PASS) as slow release oxidant to remediate phenol-contaminated groundwater

Maneekarn Yoo-iam,[1] Tunlawit Satapanajaru,[1] Chanat Chokejaroenrat,[1] Chainarong Sakulthaew,[2] Steve Comfort,[3] and Ann Kambhu [1]

1 Department of Environmental Technology and Management, Faculty of Environment, Kasetsart University, Bangkok, 10900, Thailand
2 Department of Veterinary Technology, Faculty of Veterinary Technology, Kasetsart University, Bangkok, 10900, Thailand
3 School of Natural Resources, University of Nebraska–Lincoln, Lincoln, NE 68583-0915, USA

Corresponding author — T. Satapanajaru, e*mail* fscitus@ku.ac.th

Abstract

The research objective was to develop a persulfate-activator soft solid (PASS) as a biodegradable slow-release oxidant to treat phenol-contaminated groundwater. PASS was prepared by graft copolymerization of acrylic acid (AA) and acrylamide (AM) onto 1% (w/v) sodium alginate mixed with 500 mg L^{-1} sodium persulfate and 5 mg L^{-1} ferrous sulfate. The physical and chemical properties of PASS were characterized using scanning electron microscopy, Fourier transform infrared spectroscopy, thermogravimetric analysis, differential scanning calorimetry, the water content and swelling ratio. Various variables, including the ratio of AA/AM, pH, temperature and the type of groundwater cations affecting PS release, were investigated. The maximum PS release in DI water was 98% in the ratio of PASS 1 (AA/AM, 75/25), 96% at pH 3, 83% at 25 °C, and 80% with Na+. The major factors controlling PS release were the AA/AM ratio and pH. PASS 1 can be stable in size and shape for 6–8 days and completely degraded within 34

Published in *Environmental Technology & Innovation* 22 (2021) 101396
doi:10.1016/j.eti.2021.101396

Submitted 12 October 2020; revised 15 January 2021; accepted 23 January 2021; published 2 February 2021.

days. The degradation rates of 10 mgL^{-1} phenol using PASS produced the highest k_{obs} values for each variable at a ratio of PASS 1 (k = 0.1408 h^{-1}), pH 7 (k = 0.1338 h^{-1}), 25 °C (k = 0.1939 h^{-1}), and Ca^{2+} (k = 0.1336 h^{-1}). The temperature of the groundwater was key to driving the reaction between PS and phenol. PASS 1 was applied in simulated phenol-contaminated groundwater via horizontal tanks containing Ottawa sand. The results indicated 93.2% phenol removal within 72 h in a narrow horizontal flow tank and 41.7% phenol removal in a wide horizontal flow tank with aeration.

Keywords: Alginate, Graft copolymerization, Groundwater remediation, Phenol, Persulfate-activator soft solid (PASS), Persulfate

1. Introduction

In general, traditional in situ chemical oxidation (ISCO) with a liquid oxidant has been well studied because it has the advantage of being a simple process for oxidant preparation, is easy to inject, and the exact concentration of oxidant is known. ISCO has been widely used for the oxidative degradation of organic pollutants, such as hexachlorocyclohexane (HCH), polycyclic aromatic hydrocarbon (PAH), total petroleum hydrocarbon (TPH), phenolic compounds, and trichloroethene (TCE) in soil and groundwater (Santos et al., 2018; Ranc et al., 2017; Satapanajaru et al., 2017; Ji et al., 2017; Liu et al., 2019). However, a limitation of using liquid oxidants is that they are not suitable for fine-textured soils and low-permeability sites (Lee and Schwartz, 2007). Furthermore, they cannot be used for oxidizing persistent plumes because liquid oxidants are relatively short lived (Evans et al., 2019). Therefore, to overcome these problems, a slow-release oxidant has been developed to replace liquid oxidants, and in addition, this oxidant can be used to treat a persistently contaminated plume by minimizing rebound and reducing the operating and maintenance costs (Christenson et al., 2012).

Various studies have reported that paraffin wax slow-release oxidants have high degradation efficacies (Christenson et al., 2016; Evans et al., 2019; Kambhu et al., 2017, 2012). However, a paraffin wax slow-release oxidant also requires many steps to remove the remaining paraffin wax after the remediation process is complete. Then, a slow-release oxidant gel (permanganate gel) was developed in fluid form to solve the problem of the intermittent oxidant release, as well as to create a relatively large and deep oxidation zone (Lee and Gupta, 2014; Lee et al., 2014). However, when dense fluid (permanganate gel) is injected into the aquifer, there is a decrease in the sinking of the oxidant and the concentration of

the oxidant due to dilution (Hawkins et al., 2017). Moreover, the problem of MnO_2 precipitation in permanganate is also encountered (Evans et al., 2019).

From the above limitations, we chose to study a soft solid oxidant (SSO) for groundwater remediation. SSO is a polymer that has a three-dimensional structure and cross-linked hydrophilic, linear, or branched polymers that are capable of swelling and retaining large volumes of water (Baki and Abedi-Koupai, 2017; Pourjavadi et al., 2008). SSO can be synthesized using many methods, such as radical copolymerization (Wang et al., 2014), frontal copolymerization (Yan et al., 2005), cross linking (Jeong et al., 2020), ionizing radiation (Sedlacek et al., 2017), and graft copolymerization (Kumar et al., 2019). Recently, graft copolymerization of vinyl monomers, such as acrylic acid (AA) and acrylamide (AM), onto backbone polysaccharides, such as starch, chitosan, or sodium alginate (NaAlg), has been a popular method because it involves simple steps, and only 2–3 chemicals are needed (Baki and Abedi-Koupai, 2017). In particular, using NaAlg as a backbone polymer has been popular because NaAlg is extracted from brown algae (Phillips and Williams, 2000). In addition, after the grafting process, a more suitable and low toxicity polymer was produced for environmental applications (Baker et al., 2009). The graft copolymerization method is useful for the synthesis of soft solid alginate (SSA) and has been applied to various tasks (Sahraei et al., 2017), such as medical applications and drug delivery, and in agriculture as a slow-release fertilizer (Chang et al., 2010). Its slow-release ability makes it suitable for use in environmental remediation purposes as a slow-release oxidant.

The objective of this research was to synthesize a slow-release persulfate oxidant, which is referred to as persulfate-activator soft solid (PASS), using graft copolymerization with acrylic acid (AA)/acrylamide (AM) onto sodium alginate (NaAlg). Ferrous irons (Fe^{2+}) were used as the activator. Then, we prepared PASS with Fe^{2+} in a simultaneous form to increase its capability and to make it suitable for use in the remediation process. The physical and chemical characteristics of PASS were investigated. The effects on the rate of PS release were also studied. The degradation efficacy of PASS was studied for treating phenol (representing an organic contaminant because phenol is used in many types of industries and subsequent contamination in groundwater has been reported) contamination in synthetic groundwater through a series of

batch experiments. Furthermore, the efficiency of treating groundwater contaminated with phenol in a simulated environment in a horizontal flow tank was studied. To compare with other oxidation methods, catalytic ozonation is high operation cost and fenton oxidation activated by ferrous ion suffers from iron sludge (Wang et al., 2012) while slow release persulfate or PASS has a relatively higher redox potential of 2.8 V with sulfate radicals forming and remains in a stable form after activation (Yoo-iam et al., 2020). Moreover, PASS produced from biodegradable materials is safe and easily decomposed. Therefore, our results can provide essential knowledge for developing a novel remedial technique using PASS in the field for ISCO remediation.

2. Materials and methods

2.1. Chemicals

All chemical reagents used in the experiments were analytical grade. The graft-copolymerization process was performed with NaAlg as the polymer backbone and was purchased from M.P. Biomedical (China). Acrylic acid (AA) and acrylamide (AM) were used as monomers. TCI America supplied the AA (USA), and the AM was supplied by Acros Organics (China). Alfa Aesar, USA, provided methylene bisacrylamide (MBA) as the cross-linking agent. Sodium persulfate ($Na_2S_2O_8$) was used as the initiator, and oxidants were provided by Merck Corp. (Germany), and anhydrous calcium chloride ($CaCl_2$), which was used as the precipitating agent, was supplied by E.M. Science (Germany). Phenol was purchased from Acros Organics (United Kingdom). Sulfuric acid (H_2SO_4, 98%), sodium hydroxide (NaOH, 99.0%) and potassium iodide (KI 99.5%) were purchased from Fisher Chemical (USA). Ferrous sulfate heptahydrate ($FeSO_4.7H_2O$) was purchased from Mallinkrodt Baker Inc. (USA). Sodium bicarbonate ($NaHCO_3$) was purchased from J.T. Baker (USA). Sodium chloride (NaCl), potassium chloride (KCl), ammonium chloride (NH_4Cl), and calcium chloride ($CaCl_2$) were used to study the influence of cations on the release and degradation of phenol with PASS and were purchased from J.T. Baker (USA).

2.2. Graft-copolymerization process for developing PASS

The graft copolymerization process was adapted from Baki and Abedi-Koupai (2017) to prepare PASS. The ratio of NaAlg to persulfate was 1:50 (1 g of NaAlg:50 g persulfate). One percent NaAlg solution was stirred at 600 rpm with a magnetic stirrer for 15 min to form a gelatinized NaAlg paste. The gelatinized NaAlg paste was added to 50 g of persulfate and mixed well, and then, AA/AM was added at a ratio of 75:25. The mixture was stirred continuously at 600 rpm for 120 min to make a PS gel suspension. Then, Fe^{2+} encapsulated in NaAlg as the activator was prepared by the method adapted from Mosmeri et al. (2017). A sample of 5 mg of Fe^{2+} from $FeSO_4$ was dissolved in a NaAlg solution (1%) and stirred for 10 min. The mixing solution was dropped into a beaker with a 2 mol L^{-1} $CaCl_2$ solution, and the drops were left in that $CaCl_2$ solution for 1 h. Then, the Fe^{2+} beads were removed from the solution and rinsed with distilled water. Fe^{2+} beads were added to the PS suspension, mixed well with a stirrer and left overnight.

2.3. Persulfate and activator soft solid (PASS) characteristics

Soft solid alginate (SSA) and PASS were characterized. The surface-functional group distributions were determined using Fourier transform infrared (FTIR) spectroscopy (BRUKER: Alpha-E). The morphology and chemical composition of SSA and PASS were examined using scanning electron microscopy (SEM) with energy-dispersive X-ray spectroscopy (EDX) (HITACHI SU5000). Thermogravimetric analysis (TGA 8000, Perkin Elmer) was carried out over a temperature range of 0–500 °C with a constant heating rate of 10 °C min^{-1} under a nitrogen atmosphere to determine the thermal degradation of SSA and PASS. The glass transition temperature (T_g) and melting temperature (Tm) were determined using differential scanning calorimetry (DSC) (Mettler Toledo). Approximately 10 mg of the sample was sealed in a standard 40 μL aluminum crucible and analyzed under nitrogen purging at a flow rate of 40 mL min^{-1}. The temperature range investigated was 0–500 °C at a heating rate of 10 °C min^{-1}. The equilibrium water content (WC) and swelling ratio (S) were studied at room temperature by cutting SSA and PASS samples into pieces (size 1 × 1 × 1 cm) and then placing them in DI water.

The equilibrium water content (WC) and swelling ratio (S) were determined using Eqs. (1) and (2), respectively:

$$WC\ (\%) = \frac{(W_s - W_0)}{W_s} \times 100 \quad (1)$$

$$S = \frac{(W_s - W_0)}{W_0} \quad (2)$$

where W_s and W_0 are the weights of the swollen and dry weights of SSA and PASS, respectively.

2.4. Stabilization experiment of SSA and PASS

The stabilization of SSA and PASS in water was studied at room temperature. The SSA and PASS were cut into a size close to 2 × 2 × 2 cm. The initial weight of each soft solid was approximately 5.0 g. Then, SSA or PASS was added into a 500 mL glass beaker containing 250 mL of DI water. To observe the change in weight, the SSA or PASS was taken at selected times, the excess water was removed, and the weight was measured with a 4-digit electronic balance.

2.5. PS release from PASS in water

Five grams of PASS (piece size 2 × 2 × 2 cm) containing 50 mg PS and 0.05 mg Fe^{2+} was added to a flask containing 250 mL of DI water. After allowing time for equilibration, the samples were collected and measured using the iodometric method developed by Liang et al. (2008). The calibration curve was constructed by preparing a standard solution of various sodium persulfate stock solutions. A 0.1 ml sample solution was added to 40 mL DI water and mixed well. Then, 0.2 g sodium bicarbonate was added to the solution to prevent oxidation of the iodide, and 4 g of potassium iodide was added. The resulting solution was hand shaken and allowed to equilibrate for 15 min. Then, the absorbance of each sample was measured using a spectrophotometer at 400 nm. The sodium persulfate concentration in the sample solution was calculated based on Eq. (3):

$$C_{Na_2S_2O_8}\ (mg\ L^{-1}) = C_{Cal}\ DF \quad (3)$$

where $C_{Na_2S_2O_8}$ is the concentration in the sample solution, C_{cal} is the concentration in the measurement solution in the calibration curve, and DF. is the dilution factor.

The effects of the AA/AM ratio, pH, temperature, and type of cation on PS release were studied. The parameters investigated were as follows: ratios of AA and AM of 75:25 (PASS 1), 50:50 (PASS 2), and 25:75 (PASS 3); initial pH values of 3, 5, 7, and 9; five temperatures of 5, 10, 15, 20, and 25 °C; and 100 mM of four types of cations (Na^+, K^+, NH^{4+}, and Ca^{2+}).

2.6. Kinetics degradation of phenol by PASS

Synthetic groundwater was spiked with 10 mg L^{-1} phenol. Batch experiments were conducted in an Erlenmeyer flask with 100 mL of contaminated groundwater. Treatments consisted of phenol-contaminated groundwater treated with PASS or the control (no PASS). All experiments were conducted at room temperature for 12 h in triplicate. Temporal changes in residual phenol concentrations were determined, and the pseudo-first-order kinetic rates (k) of phenol oxidation by persulfate were calculated using Eq. (4):

$$C = C_o e^{-kt} \tag{4}$$

where C_o is the initial phenol concentration and C is the concentration of phenol at time (t).

To observe the effects and phenol degradation, batch experiments were conducted in a 100 mL solution that contained 10 mg L^{-1} phenol and 5 g PASS containing 50 mg PS and 0.05 mg Fe^{2+}. The ratio of AA/AM, initial pH, temperature, and type of cation were varied to observe the phenol degradation rates. The ratios of AA to AM were 25:75, 50:50, and 75:25. The initial pH values were adjusted to 3, 5, 7, and 9, five temperatures were used (5, 10, 15, 20, 25 °C), and four types of cations were considered (Na^+, K^+, NH^{4+}, and Ca^{2+}).

2.7. Phenol and Fe^{2+} analysis

Samples were placed into a 1.5 mL microcentrifuge tube. Then, 0.25 mL sodium thiosulfate (500 g L^{-1}) was added to quench the persulfate, and the reaction was stopped, followed by centrifugation for 15 min (Kambhu et al., 2012). The supernatant was transferred to a glass vial

and analyzed using high-performance liquid chromatography (HPLC). A photodiode array detector and an isocratic mobile phase of 50:50 acetonitrile-water were used with an injection volume of 20 μL. We used a flow rate of 1 mL min^{-1}, and all samples were separated using an AQUASIL C18 column. For each treatment, the removal efficiency was calculated at 12 h based on Eq. (5):

$$\text{Phenol removal efficiency}(\%) = \frac{(C_0 - C_t)}{C_0} \times 100 \quad (5)$$

where C_0 is the initial phenol concentration in the groundwater, and C_t is the concentration of phenol after treatment.

We used the phenanthroline method to determine the concentration of Fe^{2+} in all samples. Then, the concentration of Fe^{2+} was measured using a spectrophotometer at 508 nm (APHA, 1997).

2.8. Application of PASS in a simulated phenol-contaminated groundwater aquifer (horizontal tank study)

Narrow and wide rectangular acrylic tanks were used to mimic the flow of groundwater and the treatment of contaminated groundwater with PASS. Both flow tanks consisted of 3 reservoirs: inlet, main, and outlet. The panels between the main reservoir and the inlet and outlet reservoirs were drilled and covered with a stainless steel mesh to allow the solute to flow freely and to prevent the sand from leaving the main reservoir. A constant head was maintained above the drainage port in the inlet reservoir to provide the gradient needed to induce advection (**Fig. 1**).

2.8.1. Narrow horizontal flow tank

The narrow flow tank used in this study was described in Chokejaroenrat et al. (2015) and is shown in Fig. 1A. In brief, the main reservoir had internal dimensions of 70 × 30 × 3 cm and was filled with graded Ottawa sand (grain size 0.150–0.425 mm). There were 30 sampling ports on the front of the main reservoir, with each port being 5 cm vertically apart and 10 cm horizontally apart. A PVC slotted cylinder screen was located in the main reservoir 5 cm from the inlet screen. The effluent port was located 25 cm from the bottom of the outlet reservoir. Initially, the tank was saturated with 10 mg L^{-1} phenol. When the experiment

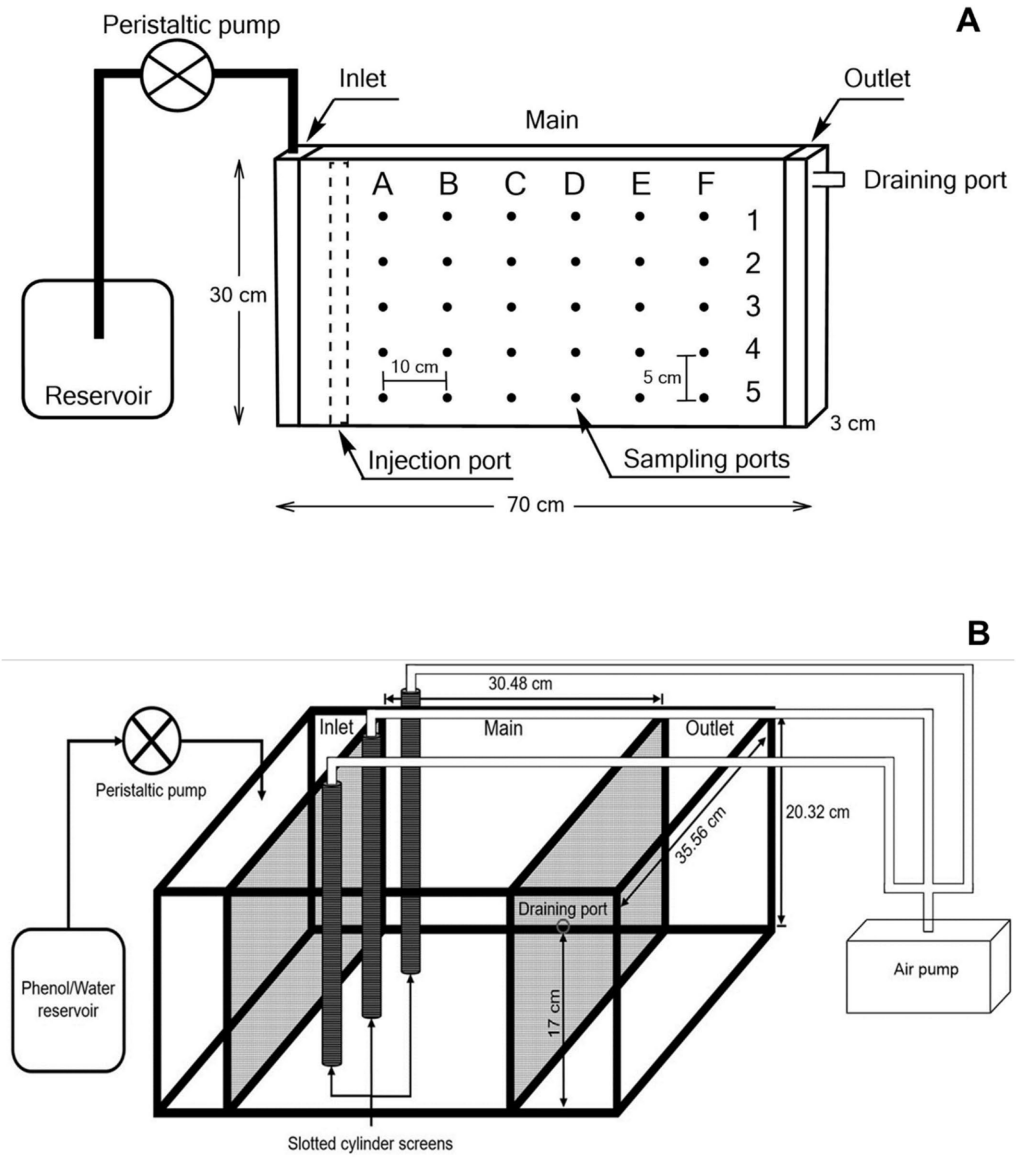

Fig. 1. Schematic diagram of the horizontal flow tank: narrow horizontal flow tank (A) and wide horizontal flow tank (B).

started, 7 pieces of PASS (each 35 g) were placed in a PVC slotted cylinder screen. The PASS used in the narrow tank experiment was cut to fit the PVC slotted cylinder screen in a rectangular block with dimensions of 1.5 × 1.5 × 4 cm. At the same time, tap water was pumped into the inlet reservoir at a flow rate of 1.5 mL min^{-1} using a peristaltic pump. Samples were collected from all 30 sampling ports at 0, 24, and 72 h.

2.8.2. Wide horizontal flow tank

The wide horizontal flow tank used in this study was described in Kambhu et al. (2021). In summary, the main reservoir had dimensions of 35.6 × 30.5 × 20.3 cm and was filled with graded Ottawa sand. The drainage port was located 17 cm from the bottom of the tank in the outlet reservoir. Three PVC slotted cylinder screens were placed approximately 7.5 cm from the inlet at the center and 8.9 cm from both sides of the center in the perpendicular direction of the flow (Fig. 1B). Similar to the narrow tank experiment, in the beginning, the system was flushed with phenol until the concentration of phenol (60 mg L^{-1}) was constant at approximately 40 L. At time zero, three rectangular pieces (each 1.5 × 1.5 × 4 cm) of PASS (each 50 g) were inserted into the PVC slotted cylinder screen, and clean water was pumped into the inlet reservoir at a flow rate of 6 mL min^{-1}. The samples were collected at the outlet reservoir every 24 h.

To determine the removal of phenol by activated liquid PS and aerated PASS, the experiment was repeated, and the mass of phenol retrieved from the outlet reservoir was compared. In the liquid PS experiment, 500 mg L^{-1} PS was injected at the same location as the PVC slotted cylinder screen. In the aerated PASS experiment, the aeration tube was connected to each PVC slotted cylinder screen at the bottom of the PVC slotted cylinder screen to improve the treatment efficiency and prevent density-driven PS release from PASS. A commercial fish tank air pump was used as an air supply, and a Cole-Parmer, 30 mm correlated flowmeter was used to control the aeration flow rate. The control treatment provided baseline phenol removal by flushing with clean water, and $CaCl_2$ was used as a tracer to provide the breakthrough curve of water. Phenol samples were collected and analyzed in the same manner as previously described. Cl^- samples were analyzed using ion chromatograph (IC).

3. Results and discussion

We synthesized SSA and PASS in square shapes (size 1 × 1 × 1 cm; 2 g, PS 500 mg and 5 mg Fe^{2+}) using a graft copolymerization method with an AA/AM ratio of 75/25. Each sample of SSA and PASS was tested for physical and chemical characteristics.

3.1. PASS characteristics

The physical and chemical properties of PASS were analyzed using SEM with EDX, FT-IR spectroscopy, TGA, DSC and for the water content and swelling ratio.

3.1.1. Scanning electron microscopy

Fig. 2 shows the SEM images of SSA and PASS (AA/AM ratio of 75/25), which were in a non-water-saturated form and ready to use. The surface of the SSA was not coarse and was relatively smooth. There were many

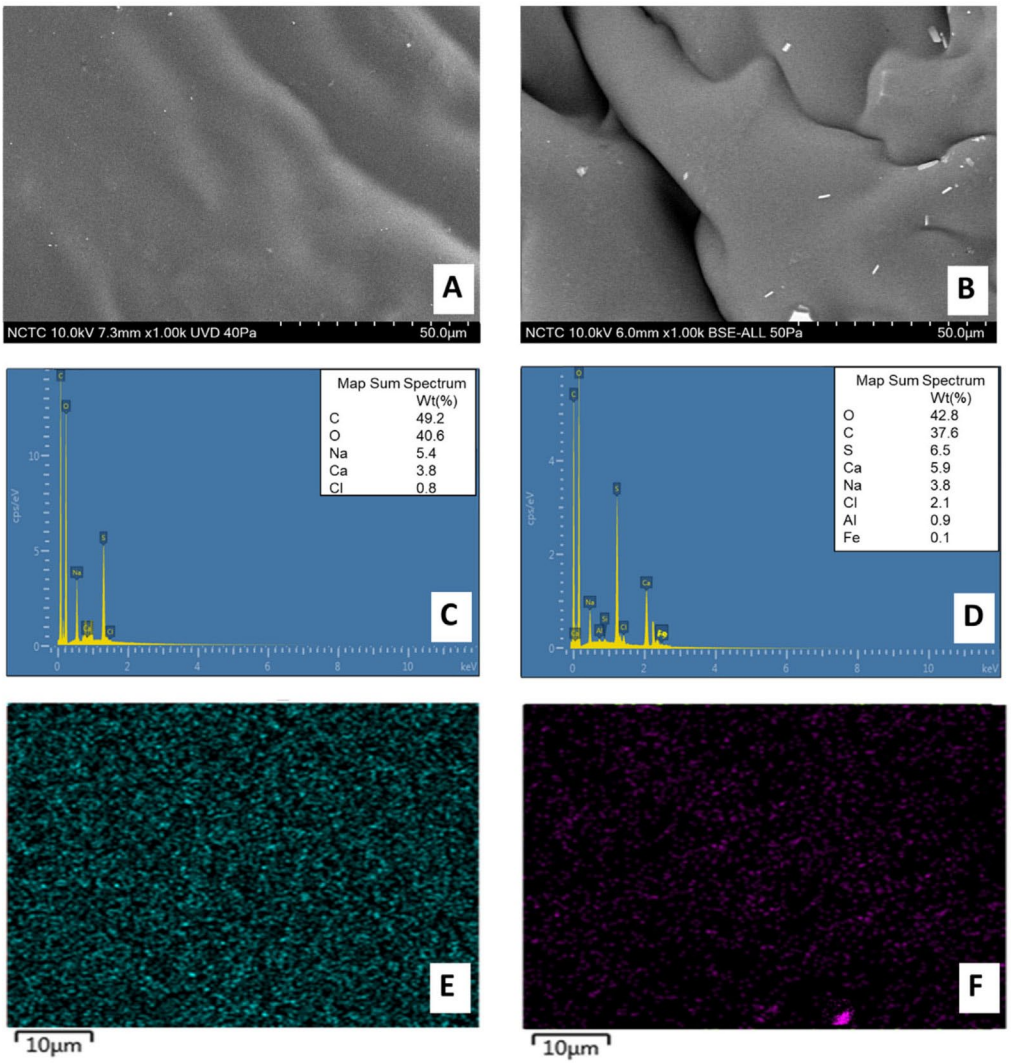

Fig. 2. SEM image of nonwater saturated SSA and PASS (AA/AM ratio of 75/25): SSA (1000x) (A) and PASS (1000x) (B), EDX result for the composition of SSA (C) and PASS (D), and the distribution of Ca^{2+} in SSA (E) and of Fe^{2+} in PASS (F).

uniform interconnected pores, as shown in Fig. 2A. These pores were regions of water permeation, where water easily diffused into the polymeric network (Kabir et al., 2018). The PASS surface was coarser than the SSA surface, as shown in Fig. 2B. PS may form an outer layer on the surface of alginate colloidal particles by electrostatic attraction, similar to the previous study by Islam et al. (2017), which reported the effect of an initiator (PS) on grafting with chitosan. The structure of PASS was more compact and disconnected than that of SSA. PASS had a coarse surface with a ridge-like structure, this uneven surface was possibly controlled-release function of PS (Tsai et al., 2017). In addition, the EDX results showed the percentage of PASS and the distribution of encapsulating Fe on PASS, as shown in Fig. 2D and F, respectively. The three major elements on the surface of PASS were oxygen (42.8%), carbon (37.6%), sulfur (6.5%), and a small amount of iron (0.1%). These results proved that the surface of PASS contained sulfur (S) and iron (Fe).

3.1.2. FTIR analysis

The surface functional groups of the SSA and PASS samples were characterized using FTIR analysis, and the FTIR spectra of the samples are presented in **Fig. 3**. Some characteristic peaks in both spectra could be identified. The observed peak at 3050–3350 cm^{-1} was attributed to the –NH stretching vibrations of AM, which overlapped with the -OH groups on the backbone (3340–3400 cm^{-1}). The peak at 2000–2120 cm^{-1} showed the C–H band, which can be present for the methyl and methylene groups of the acrylate compound (Azargohar et al., 2013). The peak at 1650 cm^{-1} corresponded to asymmetric $–COO^-$ stretching, which indicated the introduction of AA and AM into the graft-copolymer composite. The combination of a higher PS and the alginate of PASS caused an increase in the intensity of asymmetrical S═O vibration of the sulfate group present on the surface of the alginate (Fig. 3B), thus proving the interaction of PS and alginate (Singh et al., 2015). The PS-loaded PASS indicated the presence of asymmetric stretching vibrations of S–O at 1085 cm^{-1} (Kiefer et al., 2018), as shown in Fig. 3B. The peak at 575 cm^{-1} was assigned to Fe–O stretching (Santos et al., 2016). Generally, Fe^{2+} also contributes to forming a stable matrix by crosslinking with the alginate functional groups (Kang et al., 2018). Many studies of polymer–Fe complexes have shown that the carboxylic group (–COOH) of alginate forms complexes with Fe ions through hydrogen bonding with O– (Fe–O) (Dong

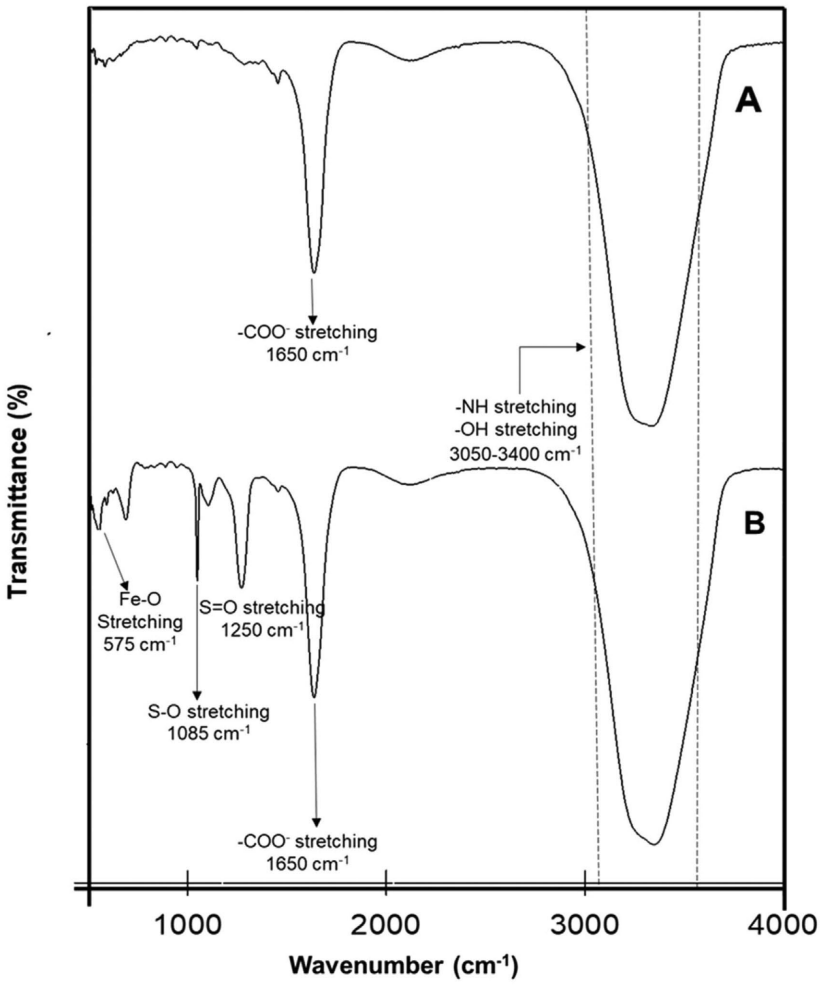

Fig. 3. FTIR spectrum of SSA (A) and PASS (AA/AM ratio of 75/25) (B).

et al., 2011; Liu et al., 2015). The results of these functional groups were related to the proposed structures of SSA and PASS (**Fig. 4**) and were in agreement with the findings regarding the loading of Fe^{2+} into PASS, as observed using EDX and SEM (Fig. 1). The changes in the spectra of PASS compared to SSA indicated interactions between the alginate and PS consisting of electrostatic interactions and noncovalent interactions, such as hydrophobic effects and hydrogen bonding (Sun et al., 2017). All the FTIR results proved that the alginate functional groups, AA, AM, PS, and Fe–O were present in the PASS spectrum.

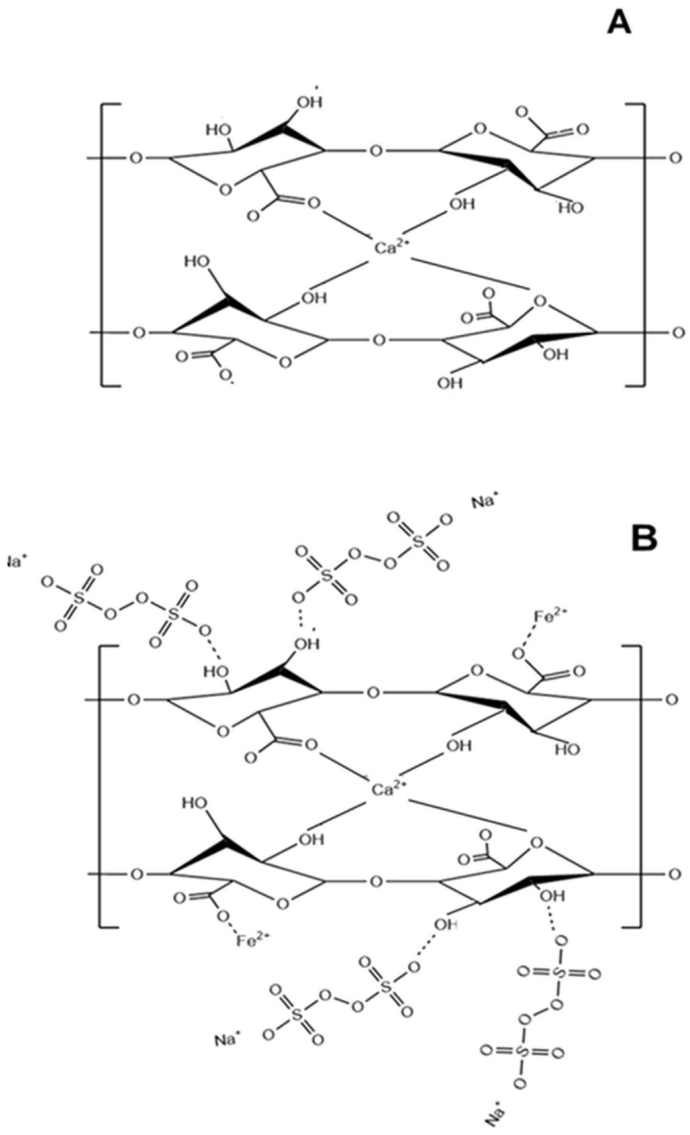

Fig. 4. The proposed structures of SSA (A) and PASS (AA/AM ratio of 75/25) (B).

3.1.3. Thermogravimetric analysis

The TGA curves of SSA and PASS are depicted in **Fig. 5**A for a heating range of 0–500 °C. The weight loss of SAA and PASS was assigned to the splitting of glycosidic bonds and desiccation of saccharide rings (Wang and Wang, 2010). The weight losses of SSA and PASS were not substantial in the low temperature range (0–100 °C). We observed that the weight loss of SSA was 86% at 140 °C, whereas PASS had a lower sample loss of 24% at the same temperature. This implies the loss of

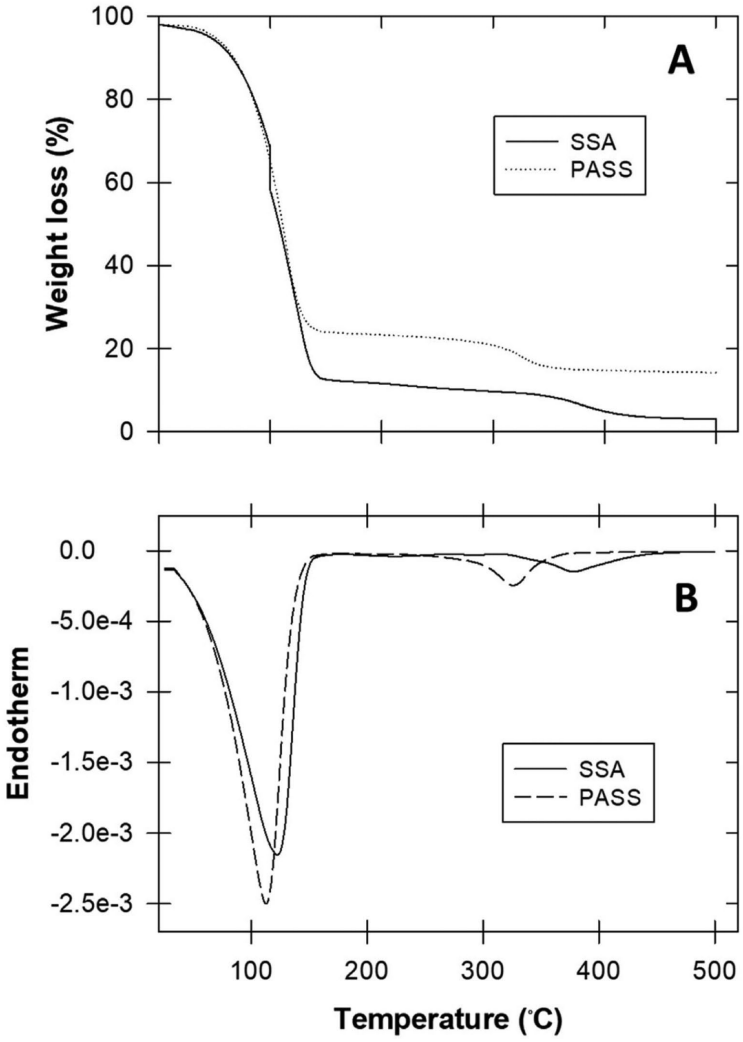

Fig. 5. Thermal gravimetric analysis (TGA) (A) and differential scanning calorimetry (DSC) (B) of SSA and PASS (AA/AM ratio of 75/25).

the cross-linked network structure and the formation of anhydride with the removal of water molecules from the carboxylic groups of polymer chains (Bao et al., 2011). At 500 °C, the thermograms of SSA and PASS had 3% and 14% residual matter, respectively. SSA had greater degradation than PASS at high temperature. The higher thermal stability of PASS may have been due to the higher PS content, which increased the number of whole cross-linked polymer groups in the grafting process (Phang et al., 2018). The TGA results revealed that PS could behave as a thermal barrier and thus increase the thermal stability of PASS.

3.1.4. Differential scanning calorimetry

The DSC results of SSA and PASS are shown in Fig. 5B. The DSC indicated traces of NaAlg endothermic peaks at 104 °C and 110 °C for PASS and SSA, respectively. Gao et al. (2009) also recorded an exothermic peak at approximately 250 °C for NaAlg. Two endothermic peaks, namely, the glass-transition temperature (T_g) and melting temperature (T_m), were clear. The exothermic peak diminished, suggesting an improvement in the decomposition temperature for NaAlg copolymers. This improvement was due to the formation of the cross-linking network. The existence of T_m indicated the formation of the crystalline region in the copolymers due to hydrogen bonding (Yong et al., 2015). The values of T_g and T_m for each copolymer are influenced by the cross-linked network formation and the strength of hydrogen bonding. Previous research showed that the initiator and cross-linking agent were activated much faster at a lower initiator concentration (Lynda Merlin and Sivasankar, 2009). Hence, in copolymers with a high concentration of initiator, more cross links could be formed in this reaction.

3.1.5. Water content and swelling ratio

The water content of SSA reached 82% within 150 min and increased to 92% within 450 min. At the same time, the PASS water content reached 60% at 150 min but did not increase until 450 min (**Fig. 6**A). The swelling ratio of SSA was ~10-fold greater than that of PASS within 450 min, as shown in Fig. 6B. The results can be explained by the fact that PS was attracted to adjoining neighbors under the grafting process, and consequently, there was a decreased distance between the alginate and monomers. The attraction force induced by adding PS reduced the diffusion of water into PASS (Kurdtabar and Bardajee, 2020). In addition, adding PS meant that there were more intermolecular interactions between the PS and alginate molecules. The polymer matrix became more compact, thus hindering water penetration, which caused the water content and swelling capacity of PASS to decrease. Furthermore, there was a high tendency for the sulfate group from PS and the carbonyl group from sodium alginate to form strong hydrogen bonds that were further responsible for a decrease in the swelling capacity (Raju and Raju, 2001; Phang et al., 2018).

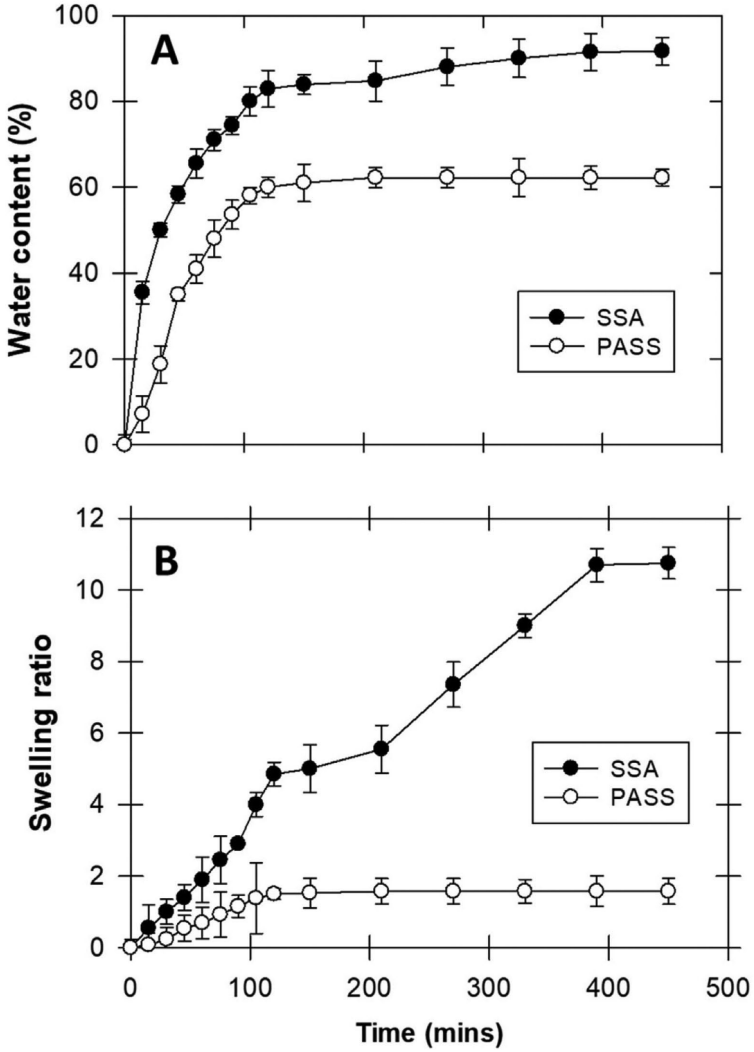

Fig. 6. Equilibrium water content (A) and swelling ratio curves for SSA and PASS (AA/AM ratio of 75/25).

3.2. Stabilization of SSA and PASS

The changes in the wet weight of SSA and PASS are shown in **Fig. 7.** The weights of SSA and PASS increased rapidly in the first stage (0–7 h). The maximum weight of SSA was as high as 60.0 g, while the weight of PASS was 12.8 g. The weights increased because of the swelling capacity and water content of SSA and PASS. A small amount of PS (0.02 g) was used as an initiator in SSA, whereas PASS contained a large amount of PS (0.5 g). PS produced free radicals in the solution, led to

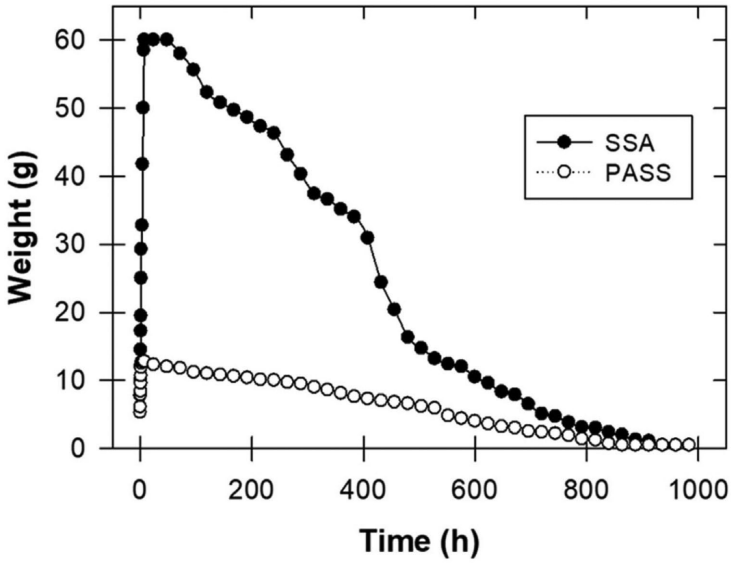

Fig. 7. The change in SSA and PASS (AA/AM ratio of 75/25) weight in water over 42 days.

more polymer graft sites and increased the swelling capacity of the SSA. However, too many free radicals shortened the graft chain of the polymer, and spatial network structures were difficult to form (Zhang et al., 2019). After 75 h, SSA and PASS were gradually degraded over time. The final weights of both SSA and PASS decreased to close to 0.5 g within 888 h (37 days). This resulted from the depolymerization of polysaccharides via cleavage of the glycosidic bonds. The glycosidic linkages of alginates are degraded by many mechanisms, including oxidative–reductive free-radical depolymerization (ORD) reactions and acid–alkaline hydrolysis (Pawar and Edgar, 2012). Thermal degradation was the main factor of alginate backbone polymer degradation; however, at low temperatures, such as in groundwater aquifers, alginate degradation did not differ significantly between effective temperature regimes of 20°C and 30 °C (Wilske et al., 2014). Our results indicated that PASS can be stable in size and shape for 6–8 days in DI water, but periods of PASS stabilization may be shortened when it is applied in the field. PASS can be degraded by microbes living in the soil and groundwater. The enzymatic degradation of microbes can decompose alginate-based polymers with morphological observations, for example, making some holes and weak topographical spots on the surface of the polymer material (Phang et al., 2018).

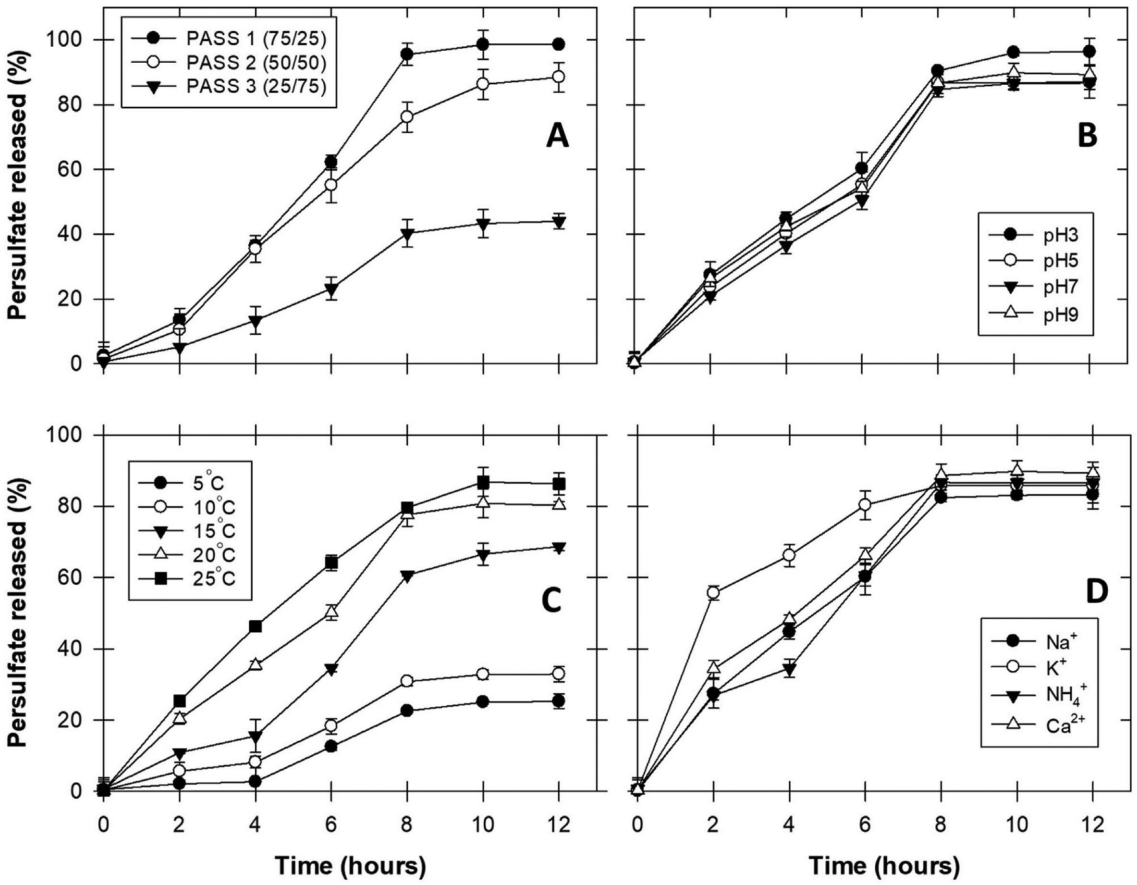

Fig. 8. Effect of PS released from PASS: AA/AM ratio (A), pH (B), temperature (C), and type of cations (D).

3.3. PS release from PASS

The possible mechanism of chemical release from the grafting polymer was based on electrostatic interactions, diffusion, and macromolecular relaxation of polymeric components in the grafted polymer (Fan et al., 2019; Faishol et al., 2019). We studied the impact of differing AA/AM ratios, pH levels, temperatures, and the type of groundwater cations on PS release from PASS. The PS release trends are shown in **Fig. 8**, and the release rate for each parameter is presented in **Table 1**.

The PS release behavior of the grafted PASS polymers with 3 different AA/AM ratios in distilled water at room temperature is shown in Fig. 8A. The PS release percentage was initially rapid and slowed down gradually. The PS release rates from PASS 1 (AA/AM ratio of 75/25), PASS 2

Table 1. PS released rate at each condition.

Parameter	*PS release rate (mg PS h^{-1})*						
	2 h	*4 h*	*6 h*	*8 h*	*10 h*	*12 h*	*24 h*
AA/AM ratio							
PASS 1 (75/25)	3.376	5.725	6.422	8.333	0.750	0.000	0.000
PASS 2 (50/50)	2.626	6.225	4.922	5.255	2.527	0.550	0.005
PASS 3 (25/75)	1.306	2.042	2.461	4.262	0.750	0.175	0.015
pH							
3	6.847	4.336	3.874	7.542	1.408	0.055	0.004
5	5.909	4.134	3.781	7.878	0.004	0.023	0.000
7	5.222	3.916	3.510	8.514	0.474	0.023	0.000
9	6.587	3.985	2.960	8.121	0.794	0.133	0.033
Temperature							
5 °C	0.522	0.151	2.464	2.495	0.625	0.055	0.005
10 °C	1.409	0.634	2.531	3.128	0.495	0.023	0.003
15 °C	2.722	1.166	4.760	6.514	1.474	0.523	0.000
20 °C	5.087	3.735	3.710	6.871	0.794	0.003	0.000
25 °C	6.337	5.235	4.460	3.871	1.794	0.026	0.006
Type of cations							
K^+	6.847	4.336	3.874	5.542	0.158	0.055	0.001
Na^+	13.909	2.634	3.531	1.378	0.004	0.023	0.003
NH^{4+}	6.722	1.916	6.510	6.514	0.025	0.023	0.000
Ca^{2+}	8.587	3.485	4.460	5.621	0.294	0.133	0.000

(AA/AM ratio of 50/50), and PASS 3 (AA/AM ratio of 25/75) increased from 2 h, and the highest release rates were at 8 h, with 8.333 mg PS h^{-1}, 5.255 mg PS h^{-1}, and 4.262 mg PS h^{-1}, respectively, as shown in Table 1. PS release started with dissolution after water had penetrated the pores (Baki and Abedi-Koupai, 2017). Initially, PS release was rapid because there was a difference between the PS concentration in the PASS and in the solution. This could be attributed to the difference in electrostatic interactions between alginate and PS (Fan et al., 2019). In addition, Fig. 8A shows that the PS release rate from PASS decreased with an increasing AM concentration. The grafted polymers were classified according to the molar ratio of AA to AM with AA/AM ratios of 75:25 (PASS 1), 50:50 (PASS 2), and 25:75 (PASS 3). The grafted polymers with a high AM concentration had lower free water absorbency (Baki and Abedi-Koupai, 2017). Free water absorbency is dependent on the hydrogen bonding interaction between the functional groups of the polymer (Wu

et al., 2012). Once the free water absorbency decreased, it was harder for water to penetrate the PASS surface to dissolve PS, which may have decreased the PS release in our experiment.

The PS release from PASS was tested at pH levels of 3, 5, 7, and 9 (Fig. 8B), and there were no significant differences. However, Table 1 shows that there was a high PS release rate for each pH level in the first 2 h, and then release rate decreased at 4 h for all pH levels. Initially, the highest release rate was at pH 3 of 6.847 mg PS h^{-1}, which indicated that acidic conditions forced the PS to be released in an acid–base interaction (Faishol et al., 2019). Furthermore, under strongly acidic conditions, the transformation of PASS carboxyl groups into –COOH decreased the repulsive forces between PS and the carboxyl groups, resulting in lower PS release. Additionally, the formation of –COOH at low pH enhanced the hydrogen bonding interactions, which had a negative effect on PS release.

The percentages of PS released at different temperatures (5–25 °C) are presented in Fig. 8C. The lowest PS release was at 5 °C (22%), while the highest was at 25 °C (84%) and was 6.337 mg PS h^{-1} in the first 2 h, and then this release decreased gradually (Table 1). Kim et al. (2002) reported the temperature dependence of the grafting polymer when the temperature increased from 20 to 50 °C. The surface and bulk-grafted polymer decreased dramatically between 30 and 35 °C. In our case, the temperature range was low (5–25 °C). We found that at 5–15 °C, the shape of PASS was smaller and may not have reduced the size of the pores, which caused a reduction in PS diffusion and lowered the PS release efficiency.

We also studied the effect of groundwater cations on the PS release properties of PASS. In the first period, the percentage of PS release with Na^+ was higher than that for other ions (Fig. 8D). In fact, the highest PS release rate was with Na^+ at 2 h (13.909 mg PS h^{-1}). The structures of PASS were also sensitive to the strong electrostatic interactions caused by the cations present in the solution (Bao et al., 2011). PS dissolution improves with increasing cation content in the solution (Phang et al., 2018). The cations readily form a bond with the O–H group from water molecules due to their high solubility property, thus increasing the interaction for dissolution to occur (Ismail Ahmad et al., 2014). The effect of different types of cations on PS release was ordered as follows: $Na^+ > K^+ > NH^{4+} > Ca^{2+}$. The PS release was higher when subjected to monovalent cations than bivalent cations. Regarding the order of $Na^+ > K^+$, the

PS release was dependent on the size of the monovalent cation. Na^+ ions, which are a smaller than K^+, could enter the polymer network more easily, causing a decreasing osmotic pressure difference and resulting in a faster PS release rate (Lohmousavi et al., 2020). The Ca^{2+} ions also entered the grafted polymer matrix and produced complexes with the carboxyl groups of PASS, resulting in a greater degree of cross linking and, consequently, slower PS release (Lohmousavi et al., 2020). However, the ion exchange between H^+ and Ca^{2+} in solution contributed to the relaxation of the structure. The concentration of Ca^{2+} ions in solution leads to the loosening of the structure and still allows the release of PS (Nithitanakool et al., 2013).

The overall trend of PS release for each AA/AM ratio was slow in the first 2 h and then increased gradually until the highest PS release rate was at 8 h. In contrast, for pH, temperature, and the type of groundwater cations, the first 2 h produced higher PS release rates. For all experiments, after 10 to 24 h, there were very low PS release rates. The oxidant release from other materials, such as persulfate paraffin wax rods (Liang and Chen, 2017) and permanganate gel (Lee et al., 2014), was reported to be initially high and then rapidly decreased with the time of testing. The differences in oxidant release of different materials may be due to their different tendencies to affect coating material properties such as the pore size. The pore size of slow-release materials depends on the type of oxidant added (Yu et al., 2014). A slow-release oxidant made from wax appeared to have very low dissolution (Lee et al., 2008). On the other hand, wax coating on the oxidant had the disadvantage of retaining residual amounts of oxidant. This may pose both economic and environmental challenges (Ibrahim and Jibril, 2005). In reference to slow-release permanganate gel made from colloidal silica, colloidal silica is a dense fluid that causes undulations at the boundaries between the high-conductivity layer and the low-conductivity layer after injection. Pooling, instabilities, and subsequent sinking of the oxidant further down were found.

3.4. Comparison of liquid PS and PASS efficiency

Substantial removal of phenol was observed with both oxidants (liquid PS and PASS 1), as shown in **Fig. 9**A, indicating that the PS slowly released from PASS was able to oxidize a substantial amount of phenol (up

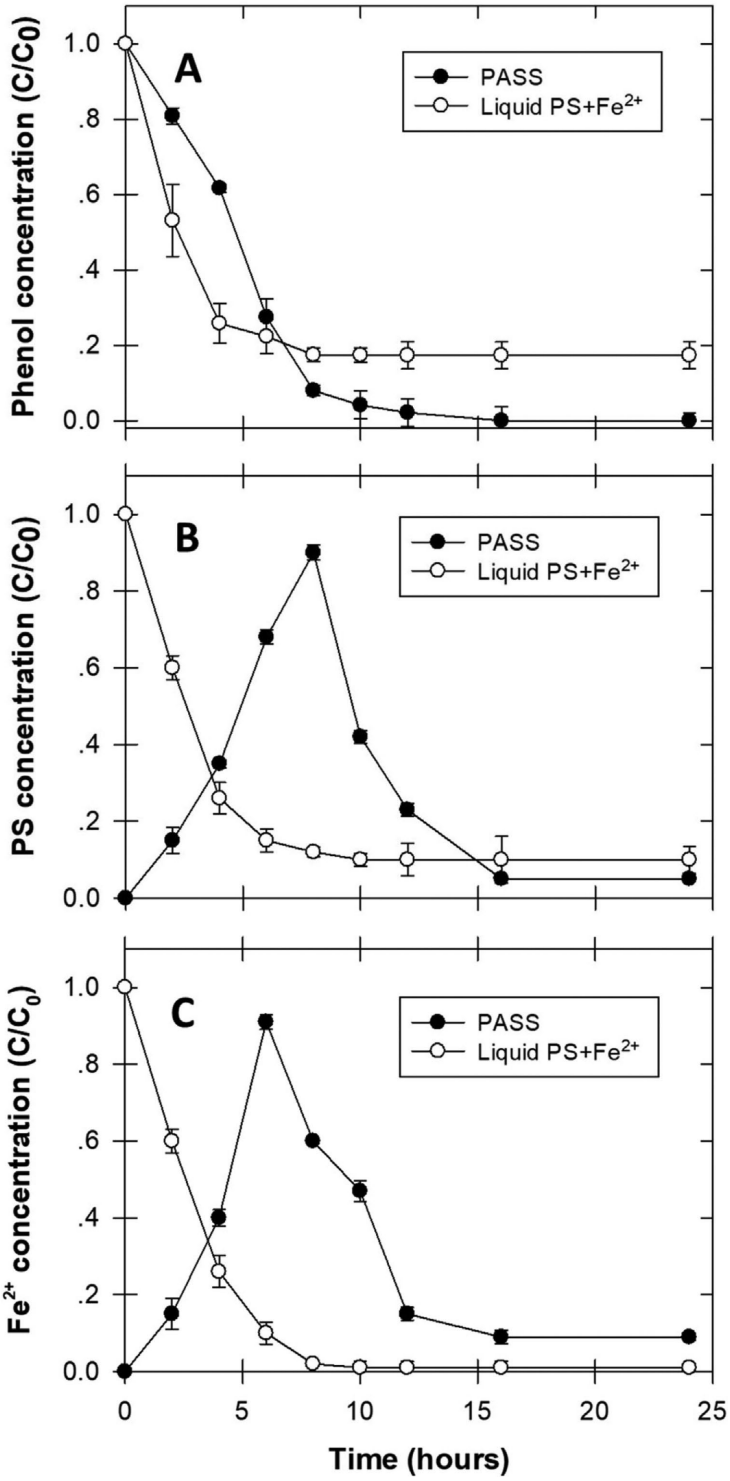

Fig. 9. Phenol removal efficiency (A), PS release concentration (B), and Fe^{2+} concentration (C) of PASS 1 and liquid PS with Fe^{2+}.

to 100%) within 24 h. The changes in the persulfate and ferrous concentrations are shown in Fig. 9B and C, respectively. The results of comparing the phenol removal efficiency between liquid PS and PASS showed that in the early stage (0–6 h), liquid PS had a faster degradation rate than PASS; then, the pattern for liquid PS plateaued at 8 h (82% phenol removal), while PASS was able to treat phenol up to nearly 100%. After 8 h of liquid PS treatment, there were insufficient ferrous ions for the activation of persulfate oxidation, and the reactions appeared to stop. On the other hand, PS and Fe^{2+} were still released from PASS, and the degradation reaction proceeded until all the phenol was removed.

We prepared PASS with Fe^{2+} as an activator that helped increase the phenol removal efficiency. When Fe^{2+} is used to activate persulfate, Fe^{2+} can be oxidized and transformed into ferric iron (Fe^{3+}), which reacts with water and forms $Fe(OH)_3$ through hydrolysis (Yang et al., 2020). Furthermore, during the persulfate activation process, the produced $SO_4^{-\bullet}$ can proceed either in the recombination mechanism with other molecules or inhibit excess persulfate oxidation (Matzek and Carter, 2016; Chen et al., 2018). During the catalytic reaction, more sulfate radicals could be produced, and thus, the phenol removal efficiency could be enhanced. Our results revealed that the Fe^{2+} activator played an important role in phenol oxidation, which could result in more than 80% phenol removal within 12 h. The enhancement of phenol oxidation was exerted by the Fe^{2+} activator, which produced a higher redox potential of persulfate radicals (E_0 = 3.1 V) than that without Fe^{2+} catalysis (Ranc et al., 2016).

Although ferrous ions are able to activate the persulfate oxidation process, excessive ferrous ions might act as intrinsic scavengers of sulfate radicals (Eq. (6)) (Kolthoff and Miller, 1951) and decrease the sulfate radical concentration.

$$Fe^{2+} + SO_4^{-\bullet} \rightarrow Fe_3^{+} + SO_4^{2-} \quad (6)$$

Researchers have indicated that the destruction of sulfate radicals might occur in the presence of excess Fe^{2+} due to the rapid conversion of Fe^{2+} to Fe^{3+}, which would limit the ultimate oxidizing capability (Satapanajaru et al., 2015). Thus, the decrease in phenol oxidation efficiency was due to the effects of excess ferrous iron limiting the oxidizing capability (Yoo-iam et al., 2020).

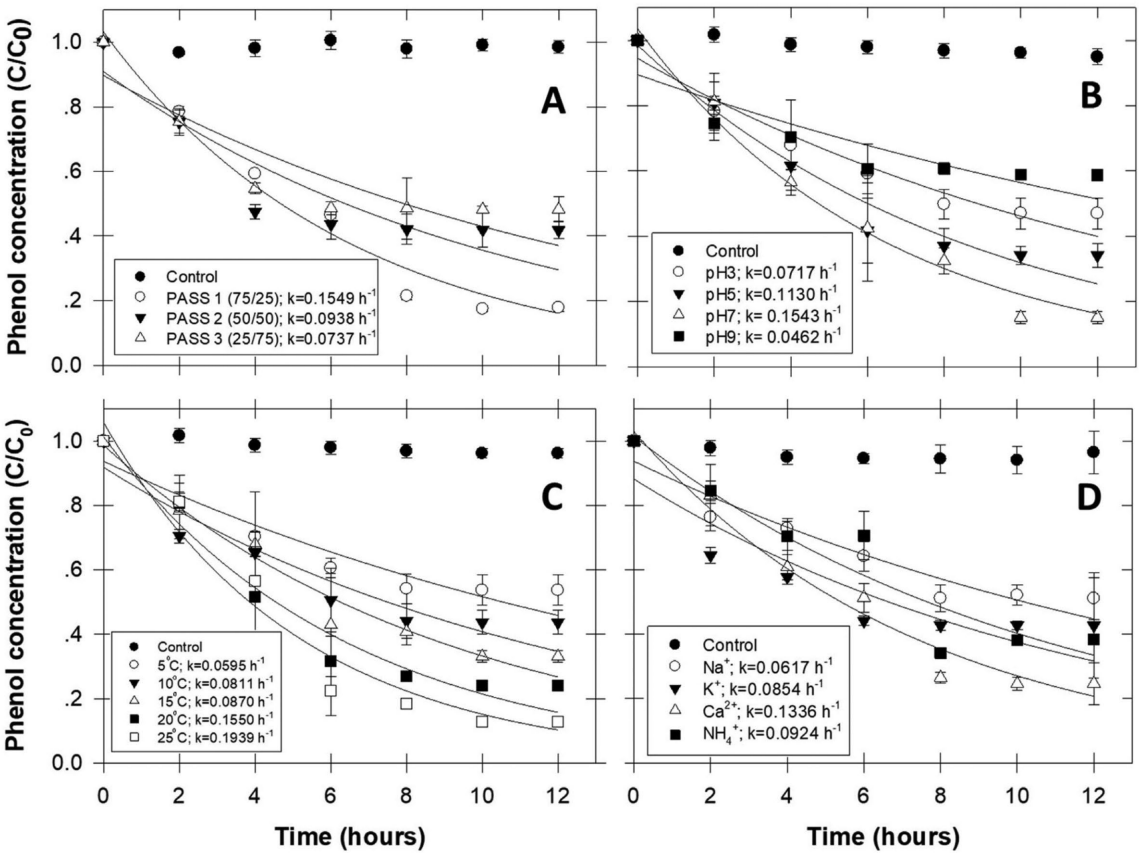

Fig. 10. Effect of phenol degradation of PASS; ratio of AA/AM (A), pH (B), temperature (C), and type of cation (D).

3.5. Effect of environmental conditions on phenol degradation by PASS

The effects of the AA/AM ratio, pH, temperature, and type of groundwater cation on phenol degradation were investigated. Three different PASS AA/AM ratios were studied in terms of phenol degradation. The k_{obs} values of the PASS 3 ratios were PASS 1 k_{obs} = 0.1549 h^{-1}, PASS 2 k_{obs} = 0.0938 h^{-1}, and PASS 3 k_{obs} = 0.0737 h^{-1} (**Fig. 10**A). The release rate of PS from PASS was higher with a low concentration of AM. Higher PS concentrations released from PASS would be more effective in phenol degradation. The phenol removal efficiency depended on the persulfate concentration. Our results showed that the phenol removal efficiency relatively increased with the persulfate concentration released from PASS.

The efficiency of PS-based AOP technologies is generally dependent on the initial pH of the solution (Yang et al., 2014). The influence of the initial pH on phenol removal in synthetic groundwater by PASS 1 (AA/AM, 75/25) was investigated over a wide range (pH 3–9, no buffer). As shown in Fig. 10B, the k_{obs} values at pH 3, 5, 7, and 9 were 0.0717 h^{-1}, 0.1130 h^{-1}, 0.1543 h^{-1}, and 0.0462 h^{-1}, respectively. Phenol degradation was best at neutral pH (pH = 7; k_{obs} = 0.1543 h^{-1}). In general, the degradation effect of the phenol solution was greatly affected by the pH value (Bing and Wei, 2019). In this work, pH 7 was the optimum pH value of the reaction, and the removal rate of phenol had a maximum efficiency of 81.72%. As the pH increased (from pH 7 to pH 9), the degradation of phenol decreased, and the removal rate of phenol gradually decreased. The pKa of SO_4^{2-} was 9.4, so SO_4^{2-} was assumed to be the only species in solution under neutral and acidic conditions (pH 3, 5, and 7), while a small amount of SO_4^{2-} was in the solution under alkaline conditions (pH 9) (Guan et al., 2011). Other researchers have observed that better pollutant removal was achieved under acidic conditions in different sulfate-radical-based systems (Jiang et al., 2016; Li et al., 2017). PS has a substantially acidic nature, and the pH of the solution containing phenol and peroxydisulfate was approximately 7 (Zhao et al., 2020).

The phenol degradation efficiency increased substantially with pH under acidic and neutral conditions, indicating that a lower pH was favorable to degrade phenol. This result was consistent with previous reports about the sulfate radical-based oxidation of fluoroquinolone (Jiang et al., 2016) and triclosan (Gao et al., 2016). This phenomenon could be explained by the predominant radical species being affected by the solution pH (Zhao et al., 2019). The current study also produced a higher reaction rate under neutral conditions than under acidic conditions. Zhao et al. (2020) reported a similar result, with the removal efficiencies of phenol by persulfate oxidation being higher under neutral conditions because the sulfate radical had a high standard redox potential (2.5–3.1 V) under acidic and neutral conditions (Zhang et al., 2015). We found a decrease in the phenol degradation rate at pH 9 due to the reaction of $SO_4^{-\bullet}$ with OH– to SO_4^{2-} and the $HO^{\cdot -}$ form (Neta et al., 1988). The $SO_4^{-\bullet}$ formed may have reacted with H_2O or OH^- to generate OH under basic pH conditions following Eqs. (7) and (8), respectively (Zhang et al., 2013):

$$\text{All pH values} : SO_4^{-\bullet} + H_2O \rightarrow SO_4^{2-} + {}^{\bullet}OH + H^+ \quad (7)$$

$$\text{Alkaline pH} : SO_4^{-\bullet} + OH^- \rightarrow SO_4^{2-} + {}^{\bullet}OH + H^+ \quad (8)$$

Hydroxyl radicals have a lower standard reduction potential than sulfate radicals under basic conditions (Anipsitakis and Dionysiou, 2004). Moreover, the Fe^{2+} concentration may have decreased at pH 7 to 9 due to iron oxide formation, which hindered the Fe^{2+} and PS reaction (Li et al., 2020).

Temperature is another variable that influences catalyst activity and phenol degradation (Zhao et al., 2020). The degradation efficiencies of phenol by PASS 1 (AA/AM, 75/25) at 12 h and 5 °C, 10 °C, 15 °C, 20 °C, and 25 °C were the following: 42.63%, k_{obs} = 0.0595 h^{-1}; 60.35%, k_{obs} = 0.0811 h^{-1}; 78.08%, k_{obs} = 0.0887 h^{-1}; 80.54%, k_{obs} = 0.1550 h^{-1}; and 90.87%, k_{obs} = 0.1939 h^{-1}, respectively (Fig. 10C). As the temperature increased, the degradation efficiency of phenol continued to increase. This result was attributed to a portion of the energy generated by the system participating in the activation of the oxidant, which produced more sulfate radicals and improved the degradation efficiency of phenol (Pan et al., 2018). Adverse effects have been reported owing to the competitive consumption of radicals at high temperature and the diffusion limitation phenomenon (Xu and Wang, 2012).

Gibbs free energy (ΔG^0) values can be evaluated using Eq. (9) at various temperatures (Ahmadi et al., 2019):

$$\Delta G^0 = - RT \ln k \quad (9)$$

where R is the universal gas constant (0.0083 kJ mol^{-1}), T is the solution temperature (K), and k is the kinetic rate constant.

The ΔG^0 values for phenol degradation in this study at 5 °C, 10 °C, 15 °C, 20 °C, and 25 °C were −4.059 kJ mol^{-1}, −4.536 kJ mol^{-1}, −5.793 kJ mol^{-1}, −5.903 kJ mol^{-1}, and −6.514 kJ mol^{-1}, respectively. The basic principle is that degradation spontaneity must be negative when ΔG^0 changes for suitable degradation to exist (Yan et al., 2017). The negative ΔG^0 values showed that the PS process was simple and that the level of spontaneity of the reaction increased with increasing temperature (Ahmadi et al., 2019). This result supported that the reaction mechanism was strongly stable and that the rate of the PS oxidation reaction increased with increasing temperature.

The effects of groundwater cations (K^+, Na^+, NH^{4+}, and Ca^{2+}) on phenol degradation by PASS 1 (AA/AM, 75/25) are shown in Fig. 10D. The k_{obs} values for all the cations were between 0.0617 and 0.1336 h^{-1}; these K_{obs} values were not very good for treating phenol, perhaps because the combination of these cations with SO_4^{2-}, generated from $S_2O_8^{2-}$, results in low efficiency of phenol removal. The presence of cations showed their influence on the oxidation ability of the oxidant in the Fenton-combined persulfate system (Li et al., 2018). When cations were present, the generation of sulfate radicals decreased substantially, suggesting that the existence of these cations that we studied could decrease the oxidative capacity of the oxidation process. On the other hand, the transition metal cation was effective at activating PS in the oxidation process. Anipsitakis and Dionysiou (2004) presented various charges of metal catalysts, including Ag^+, Co^{2+}, Fe^{2+}, Mn^{2+}, Ni^{2+}, Ce^{3+}, and Ru^{3+}, for the activation of persulfate and peroxymonosulfate to produce sulfate and hydroxyl radicals. Another study confirmed that metal ions (Co^{2+}, Fe^{2+}, Mn^{2+}, Cu^{2+}) and the mixing of these metals could activate persulfate (Ahn and Yun, 2019).

3.6. Horizontal flow tank study

A narrow flow tank experiment was conducted to study the spreading and transport of PS from PASS 1 (AA/AM, 75/25). In addition, the removal of phenol by PS in a constant flow sand tank was studied. The remaining PS and phenol concentrations in the flow tank at 24 and 72 h are shown in **Fig. 11**. At 24 h, the highest PS concentration (445 mg L^{-1}) was near the PASS screen; further away from the PASS, there were lower concentrations. The lowest PS concentration (60 mg L^{-1}) was observed near the outlet (Fig. 11A). The PS distribution indicated that the PS was released in the zone around the screen and downward in the tank (density driven), similar to Chokejaroenrat et al. (2015). With a flow rate of 1.5 mL min^{-1}, the advection front of PS reached only half the tank. Eventually, at 72 h, PS was distributed throughout the tank water (Fig. 11B).

On the other hand, the remaining phenol concentration at 24 h (Fig. 11C) was inversely related to the PS concentration (Fig. 11A) due to the degradation of phenol by the released PS. Approximately 49.7% of the phenol removal had occurred at 24 h (Fig. 11C), while at 72 h, phenol removal reached 93.2%, and the remaining phenol was found at the bottom of the tank near the outlet (Fig. 11D). The interaction zone

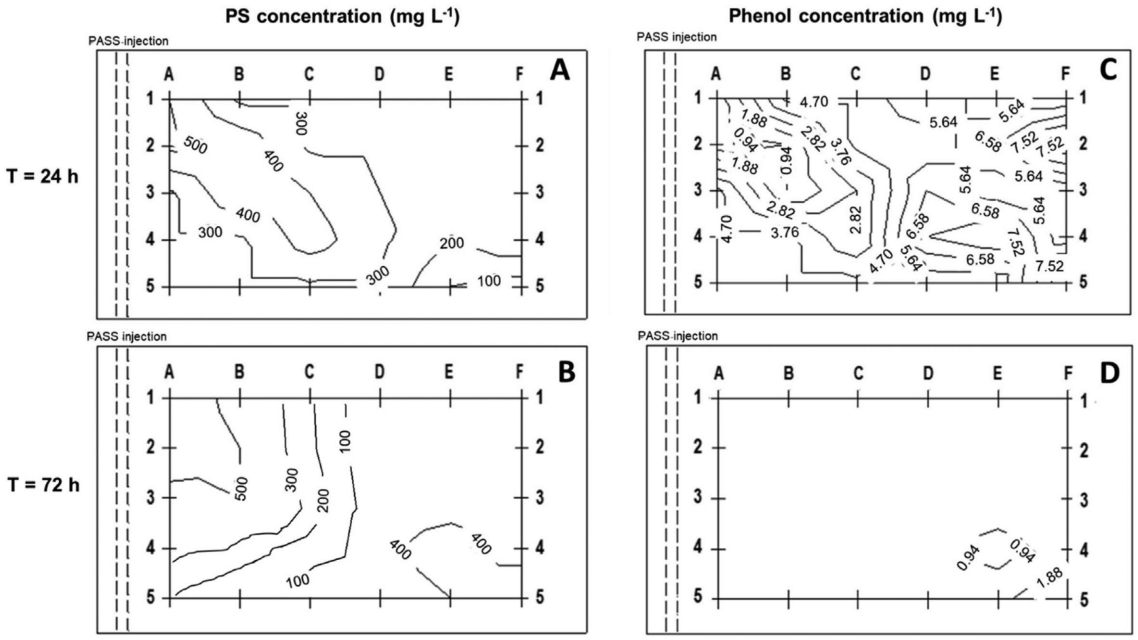

Fig. 11. Releasing of PS at 24 h (A), releasing of PS at 72 h (B), spatial phenol concentration at 24 h (C), and spatial phenol concentration at 72 h (D) in narrow horizontal flow tank when treated with PASS 1.

between sulfate radicals and phenol was produced while phenol was pushed along the tank. This revealed that the release of PS from PASS was able to successfully oxidize phenol in the downgradient area. Moreover, no flow rate or a flow rate of 1.5 mL min^{-1} resulted in greater contaminant oxidation of persulfate, while higher flow rates resulted in the advection effect being sufficient to result in substantial contaminant removal from the tank (Chokejaroenrat et al., 2015).

Furthermore, we observed the release of PS from PASS, with PS sinking when PASS was submerged in the water or placed in a permeable aquifer such as sand. This phenomenon was similar to that observed by many researchers (Christenson et al., 2012, 2016; Kambhu et al., 2012; Liang and Chen, 2017). For this reason, to eliminate the density-driven action from PASS and to improve the treatment efficiency, a pneumatic circulator was added to the bottom with a slow-release oxidant (Christenson et al., 2012, 2016; Kambhu et al., 2021). The wide horizontal flow tank was used to compare the removal of phenol by liquid persulfate injections with and without aerated PASS under flow conditions. We assumed that the area under the control curve represented 100% of the

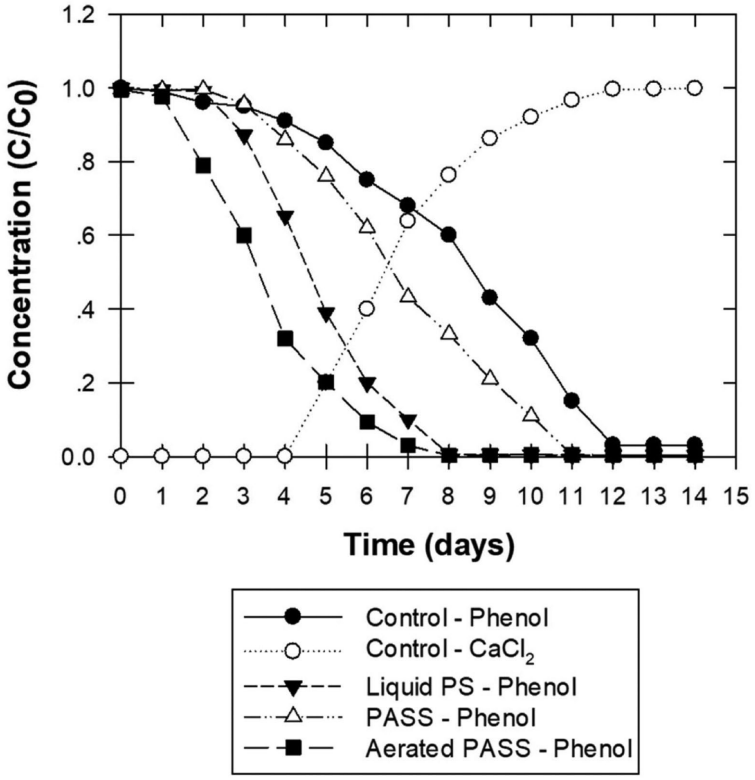

Fig. 12. Breakthrough of $CaCl_2$ and removal of phenol by flushing with water, liquid PS injection and aerated PASS 1 in the wide horizontal flow tank.

phenol available to be oxidized. We conducted the experiment by injecting liquid persulfate into a PVC slotted cylinder screen. **Fig. 12** shows the integration of the liquid PS injection treatment curves with 66.7% of the phenol recovered. The difference in phenol recovery between the control and liquid persulfate injections can be attributed to the phenol that was oxidized (up to 33.3%).

The experiment using PASS without aeration resulted in less phenol removal than with PS liquid injection, with 91.7% of the phenol recovered, indicating that 9.3% of the phenol was oxidized. We observed that at the bottom of the tank, there was some gel-like solution representing sunken persulfate. PASS 1 (50 g) was placed in the tank in the same position and then aerated. The comparison of the two treatments showed that the aerated PASS had 58.3% phenol remaining (up to 41.7% of phenol was oxidized) (Fig. 12). Aeration greatly facilitated more spreading throughout the sand in the main chamber and resulted in greater phenol oxidation (Christenson et al., 2012, 2016; Kambhu et al., 2021). Our

results indicated that the addition of PASS without aeration resulted in density-driven flow, which meant that the persulfate sank to the bottom of the flow tank. This was similar to another study that reported PS release from a slow-release paraffin wax rod that initially sank along the surface of the rod to the bottom of the rod based on visual observation (Liang and Chen, 2017). Thus, aeration is necessary to improve phenol removal efficiency.

4. Conclusions

PASS samples were made and tested on a laboratory scale. The SEM and FTIR results showed the different surface and functional groups between SSA and PASS. PS was used as an initiator and oxidant and was affected by the water content and swelling ratio. The PS release behavior was investigated in distilled water. The PS release rate experiments showed good release results within 12 h. Early in the experiment, the initial release rate was high before slowing and being sustained with time. The release behavior of the PS release was affected by the AA/AM ratio, pH, temperature, and type of cation. The highest PS release percentage was under conditions of PASS 1 (AA/AM = 75/25), a solution pH of 7 at 25 °C, and with the solution containing Na^+ ions.

PASS samples were tested under batch and transport conditions to evaluate the sustainable release of activated PS and its ability to degrade phenol in solution. The degradation results showed that the activated PS was able to degrade up to 90% of the phenol in 12 h under batch conditions, while 93.2% removal was observed within 72 h in the narrow horizontal flow tank and 41.7% in the wide horizontal flow tank with aeration. Based on these results, PASS was effective at the removal of phenol in a batch experiment and is suitable for use in the environment.

* * * *

CRediT authorship contribution statement

Maneekarn Yoo-iam: Investigation, Formal analysis, Validation, Writing - original draft.
Tunlawit Satapanajaru: Conceptualization, Methodology, Supervision, Resources, Writing - review & editing.
Chanat Chokejaroenrat: Data curation, Writing - review & editing.
Chainarong Sakulthaew: Data curation, Writing - review & editing.
Steve Comfort: Supervision, Resources.
Ann Kambhu: Data curation, Writing - review & editing.

Competing interest The authors declare that they have no known competing financial interests or personal relationships that could have appeared to influence the work reported in this paper.

Acknowledgments We acknowledge financial support from the Thailand Research Fund through the Royal Golden Jubilee Ph.D. Program (Grant No. PHD/0010/2557) to Miss Maneekarn Yoo-iam and Assoc. Prof. Dr. Tunlawit Satapanajaru. We are grateful for support from the Kasetsart University Research and Development Institute (KURDI), Bangkok, Thailand. The Department of Environmental Technology and Management, Faculty of Environment, Kasetsart University, and the Soil Chemistry Laboratory, University of Nebraska-Lincoln, provided the research area and all equipment.

References

Ahmadi, S., Adaobi, C., Somayeh, I., 2019. The application of thermally activated persulfate for degradation of acid blue 92 in aqueous solution. Int. J. Ind. Chem. 10, 249–260. http://dx.doi.org/10.1007/s40090-019-0188-1

Ahn, Y.Y., Yun, E.T., 2019. Heterogeneous metals and metal-free carbon materials for oxidative degradation through persulfate activation: A review of heterogeneous catalytic activation of persulfate related to oxidation mechanism. Korean J. Chem. Eng. 36, 1767–1779. http://dx.doi.org/10.1007/s11814-019-0398-4

Anipsitakis, G.P., Dionysiou, D.D., 2004. Radical generation by the interaction of transition metals with common oxidants. Environ. Sci. Technol. 38, 3705–3712. http://dx.doi.org/10.1021/es035121o

APHA, 1997. Standard Methods, 22nd ed. In: Method 3500-Fe B. ASTM D 1068-77, Iron in Water, Test Method A.

Azargohar, R., Nanda, S., Rao, B.V.S.K., Dalai, A.K., 2013. Slow pyrolysis of deoiled canola meal: Product yields and characterization. Energy Fuels 27, 5268–5279. http://dx.doi.org/10.1021/ef400941a

Baker, K.L., Langenheder, S., Nicol, G.W., Ricketts, D., Killham, K., Campbell, C.D., Prosser, J.I., 2009. Environmental and spatial characterisation of bacterial community composition in soil to inform sampling strategies. Soil Biol. Biochem. 41 (11), 2292–2298. http://dx.doi.org/10.1016/j.soilbio.2009.08.010

Baki, M., Abedi-Koupai, J., 2017. Preparation and characterization of a superabsorbent slow-release fertilizer with sodium alginate and biochar. J. Appl. Polym. Sci. 135 (45966), http://dx.doi.org/10.1002/app.45966

Bao, Y., Ma, J., Li, N., 2011. Synthesis and swelling behaviors of sodium carboxymethyl cellulose-g-poly (AA-co-AM-co-AMPS)/ MMT superabsorbent hydrogel, 84, 76–82, http://dx.doi.org/10.1016/j.carbpol.2010.10.061

Bing, W., Wei, W., 2019. Degradation phenol wastewater by heating activated persulfate, 7, 14–21, http://dx.doi.org/10.11648/j.ijema.20190701.12

Chang, C., Duan, B., Cai, J., Zhang, L., 2010. Superabsorbent hydrogels based on cellulose for smart swelling and controllable delivery. Eur. Polym. J. 46, 92–100. http://dx.doi.org/10.1016/j.eurpolymj.2009.04.033

Chen, L., Hu, X., Yang, Y., Jiang, C., Bian, C., Liu, C., Zhang, M., Cai, T., 2018. Degradation of atrazine and structurally related s-triazine herbicides in soils by ferrous-activated persulfate: Kinetics, mechanisms and soil-types effects. Chem. Eng. J. 351, 523–531. http://dx.doi.org/10.1016/j.cej.2018.06.045

Chokejaroenrat, C., Sakulthaew, C., Satapanajaru, T., Tikhamram, T., Pho-Ong, A., Mulseesuk, T., 2015. Treating methyl orange in a two-dimensional flow tank by in situ chemical oxidation using slow-release persulfate activated with zero-valent iron. Environ. Eng. Sci. 32, 1007–1015. http://dx.doi.org/10.1089/ees.2015.0110

Christenson, M.D., Kambhu, A., Comfort, S.D., 2012. Using slow-release permanganate candles to remove TCE from from a low permeable aquifer at a former landfill. Pap. Nat. Resour. Nat. Resour. 680–687. http://dx.doi.org/10.1016/j.chemosphere.2012.06.009

Christenson, M., Kambhu, A., Reece, J., Comfort, S., Brunner, L., 2016. A five-year performance review of field-scale, slow-release permanganate candles with recommendations for second-generation improvements. Chemosphere 150, 239–247. http://dx.doi.org/10.1016/j.chemosphere.2016.01.125

Dong, Y., Dong, W., Cao, Y., Han, Z., Ding, Z., 2011. Preparation and catalytic activity of Fe alginate gel beads for oxidative degradation of azo dyes under visible light irradiation. Catal. Today 175, 346–355. http://dx.doi.org/10.1016/j.cattod.2011.03.035

Evans, P.J., Dugan, P., Nguyen, D., Lamar, M., Crimi, M., 2019. Slow-release permanganate versus unactivated persulfate for long-term in situ chemical oxidation of 1, 4-dioxane and chlorinated solvents. Chemosphere 221, 802–811. http://dx.doi.org/10.1016/j.chemosphere.2019.01.075

Faishol, W., Rubiyanto, D., Chuenchom, L., Fatimah, I., 2019. Alginate-modified saponite and study for urea-slow released fertilizer application. Rasayan J. Chem. 12, 1792–1802. http://dx.doi.org/10.31788/RJC.2019.1245386

Fan, Y., Xu, J., Gao, X., Fu, X., Yang, X., 2019. Effect of alginate on the release of amide nitrogen for soilless cultivation applications. Sci. Hortic. (Amsterdam) 256, 108545. http://dx.doi.org/10.1016/j.scienta.2019.108545

Gao, H., Chen, J., Zhang, Y., Zhou, X., 2016. Sulfate radicals induced degradation of triclosan in thermally activated persulfate system. Chem. Eng. J. 306, 522–530. http://dx.doi.org/10.1016/j.cej.2016.07.080

Gao, N., Starink, M.J., Langdon, T.G., 2009. Using differential scanning calorimetry as an analytical tool for ultrafine-grained metals processed by severe plastic deformation. Mater. Sci. Technol. 25 (6), 687–698. http://dx.doi.org/10.1179/174328409X408901

Guan, Y.H., Ma, J., Li, X.C., Fang, J.Y., Chen, L.W., 2011. Influence of pH on the formation of sulfate and hydroxyl radicals in the UV/Peroxymonosulfate system. Environ. Sci. Technol. 45, 9308–9314. http://dx.doi.org/10.1021/es2017363

Hawkins, A.J., Fox, D.B., Becker, M.W., Tester, J.W., 2017. Measurement and simulation of heat exchange in fractured bedrock using inert and thermally degrading tracers. Water Resour. Res. 53, 1210–1230. http://dx.doi.org/10.1002/2016WR019617

Ibrahim, A.A., Jibril, B.Y., 2005. Controlled release of paraffin wax/rosin-coated fertilisers. Ind. Eng. Chem. Res. 44, 2288–2291. http://dx.doi.org/10.1021/ie048853d

Islam, S., Bhuiyan, M.A.R., Islam, M.N., 2017. Chitin and chitosan: Structure, properties and applications in biomedical engineering. J. Polym. Environ. 25, 854–866. http://dx.doi.org/10.1007/s10924-016-0865-5

Ismail Ahmad, S., Syed, I. Ahmed., Ravi Prasad, P., Ahmad, A., 2014. Quantitation of urea in urine by Fourier transforms infrared spectroscopy. Schol. Res. Libr. Pharma Chem. 6 (1), 90–96.

Jeong, C., Kim, Senghui, Lee, C., Cho, S., Kim, S.-B., 2020. Changes in the physical properties of calcium alginate gel beads under a wide range of gelation temperature conditions. Foods 9, 180–195. http://dx.doi.org/10.3390/foods9020180

Ji, Y., Wang, L., Jiang, M., Lu, J., Ferronato, C., Chovelon, J.-M., 2017. The role of nitrite in sulfate radical-based degradation of phenolic compounds: An unexpected nitration process relevant to groundwater remediation by in-situ chemical oxidation (ISCO). Water Res. 123, 249–257. http://dx.doi.org/10.1016/j.watres.2017.06.081

Jiang, C., Ji, Y., Shi, Y., Chen, J., Cai, T., 2016. Sulfate radical-based oxidation of fluoroquinolone antibiotics: Kinetics, mechanisms and effects of natural water matrices. Water Res. 106, 507–517. http://dx.doi.org/10.1016/j.watres.2016.10.025

Kabir, S.M.F., Sikdar, P.P., Haque, B., Bhuiyan, M.A.R., Ali, A., Islam, M.N., 2018. Cellulose-based hydrogel materials: chemistry, properties and their prospective applications. Prog. Biomater. 7, 153–174. http://dx.doi.org/10.1007/s40204-018-0095-0

Kambhu, A., Comfort, S., Chokejaroenrat, C., Sakulthaew, C., 2012. Chemosphere developing slow-release persulfate candles to treat BTEX contaminated groundwater. Chemosphere 89, 656–664. http://dx.doi.org/10.1016/j.chemosphere.2012.06.004

Kambhu, A., Gren, M., Tang, W., Comfort, S., Harris, C.E., 2017. Remediating 1, 4-dioxane-contaminated water with slow-release persulfate and zero-valent iron. Chemosphere 18807. http://dx.doi.org/10.1016/j.chemosphere.2017.02.044

Kambhu, A., Li, Y., Gilmore, T., Comfort, S., 2021. Modeling the release and spreading

of permanganate from aerated slow-release oxidants in a laboratory flow tank. J. Hazard. Mater. 403, 123719. http://dx.doi.org/10.1016/j.jhazmat.2020.123719

Kang, Y.-G., Vu, H.C., Le, T.T., Chang, Y.-S., 2018. Activation of persulfate by a novel Fe(II)-immobilized chitosan/alginate composite for bisphenol a degradation. Chem. Eng. J. 353, 736–745. http://dx.doi.org/10.1016/j.cej.2018.07.175

Kiefer, J., Stärk, A., Kiefer, A.L., Glade, H., 2018. Infrared spectroscopic analysis of the inorganic deposits from water in domestic and technical heat exchangers. Energies 11 (4), 798. http://dx.doi.org/10.3390/en11040798doi:10.3390/en11040798

Kim, J.H., Lee, S.B., Kim, S.J., Lee, Y.M., 2002. Rapid temperature/pH response of porous alginate-g-poly(n-isopropylacrylamide) hydrogels. Polymer 43, 7549–7558. http://dx.doi.org/10.1016/S0032-3861(02)00675-4

Kolthoff, I.M., Miller, I.K., 1951. The chemistry of persulfate, I. the kinetics and mechanism of the decomposition of the persulfate ion in aqueous medium. J. Am. Chem. Soc. 73, 3055–3059. http://dx.doi.org/10.1021/ja01151a024

Kumar, R., Sharma, R.K., Singh, A.P., 2019. Synthesis and characterization of cellulose based graft copolymers with binary vinyl monomers for efficient removal of cationic dyes and Pb(II) ions. J. Polym. Res. 26, http://dx.doi.org/10.1007/s10965-019-1790-9

Kurdtabar, M., Bardajee, G.R., 2020. Drug release and swelling behavior of magnetic iron oxide nanocomposite hydrogels based on poly (acrylic acid) grafted onto sodium alginate. Polym. Bull. 77, 3001–3015. http://dx.doi.org/10.1007/s00289-019-02894-w

Lee, E.S., Gupta, N., 2014. Development and characterization of colloidal silica-based slow-release permanganate gel (SRP-g): Laboratory investigations. Chemosphere 109, 195–201. http://dx.doi.org/10.1016/j.chemosphere.2014.01.020

Lee, E.S., Olson, P.R., Gupta, N., Solpuker, U., Schwartz, F.W., Kim, Y., 2014. Permanganate gel (PG) for groundwater remediation: Compatibility, gelation, and release characteristics. Chemosphere 97, 140–145. http://dx.doi.org/10.1016/j.chemosphere.2013.11.008

Lee, E.S., Schwartz, F.W., 2007. Characteristics and applications of controlled-release $KMnO_4$ for groundwater remediation. Chemosphere 66, 2058–2066. http://dx.doi.org/10.1016/j.chemosphere.2006.09.093

Lee, E.S., Woo, N.C., Schwartz, F.W., Lee, B.S., Lee, K.C., Woo, M.H., Kim, J.H., Kim, H.K., 2008. Characterization of controlled-release $KMnO_4$ (CRP) barrier system for groundwater remediation: A pilot-scale flow-tank study. Chemosphere 71, 902–910. http://dx.doi.org/10.1016/j.chemosphere.2007.11.037

Li, S., Li, W., Chen, H., Liu, F., Jin, S., Yin, X., Zheng, Y., Liu, B., 2018. Effects of calcium ion and pH on the adsorption/regeneration process by activated carbon permeable reactive barriers. RSC Adv. 8, 16834–16841. http://dx.doi.org/10.1039/c8ra01961d

Li, J., Ren, Y., Ji, F., Lai, B., 2017. Heterogeneous catalytic oxidation for the degradation of p-nitrophenol in aqueous solution by persulfate activated with $CuFe_2O_4$ magnetic nano-particles. Chem. Eng. J. 324, 63–73. http://dx.doi.org/10.1016/j.cej.2017.04.104

Li, X., Yuan, L., Zhao, L., 2020. A comparative study on oxidation of acidic red 18 by persulfate with ferrous and ferric ions. Catalysts 10 (698), http://dx.doi.org/10.3390/catal10060698

Liang, C., Chen, C.Y., 2017. Characterization of a sodium persulfate sustained release rod for in situ chemical oxidation groundwater remediation. Ind. Eng. Chem. Res. 56, 5271–5276. http://dx.doi.org/10.1021/acs.iecr.7b00082

Liang, C., Huang, C., Mohanty, N., Mohan, R., 2008. Chemosphere a rapid spectrophotometric determination of persulfate anion in ISCO. Chemosphere 73, 1540–1543. http://dx.doi.org/10.1016/j.chemosphere.2008.08.043

Liu, J., Wu, H., Lu, J., Wen, X., Kan, J., Jin, C., 2015. Preparation and characterization of novel phenolic acid (hydroxybenzoic and hydroxycinnamic acid derivatives) grafted chitosan microspheres with enhanced adsorption properties for Fe(II). Chem. Eng. J. 262, 803–812. http://dx.doi.org/10.1016/j.cej.2014.10.041

Liu, Y., Zhang, Y., Zhou, A., 2019. A potential novel approach for in situ chemical oxidation based on the combination of persulfate and dithionite. Sci. Total Environ. 693, 133635. http://dx.doi.org/10.1016/j.scitotenv.2019.133635

Lohmousavi, S.M., Abad, H.H.S., Noormohammadi, G., Delkhosh, B., 2020. Synthesis and characterization of a novel controlled release nitrogen-phosphorus fertilizer hybrid nanocomposite based on banana peel cellulose and layered double hydroxides nanosheets. Arab. J. Chem. 13, 6977–6985. http://dx.doi.org/10.1016/j.arabjc.2020.06.042

Lynda Merlin, D., Sivasankar, B., 2009. Synthesis and characterization of semi-interpenetrating polymer networks using biocompatible polyurethane and acrylamide monomer. Eur. Polym. J. 45, 165–170. http://dx.doi.org/10.1016/j.eurpolymj.2008.10.012

Matzek, L.W., Carter, K.E., 2016. Activated persulfate for organic chemical degradation: A review. Chemosphere 151, 178–188. http://dx.doi.org/10.1016/j.chemosphere.2016.02.055

Mosmeri, H., Alaie, E., Shavandi, M., Dastgheib, S.M.M., Tasharrofi, S., 2017. Bioremediation of benzene from groundwater by calcium peroxide (CaO_2) nanoparticles encapsulated in sodium alginate. J. Taiwan Inst. Chem. Eng. 78, 299–306. http://dx.doi.org/10.1016/j.jtice.2017.06.020

Neta, P., Huie, R.E., Ross, A.B., 1988. Rate constants for reactions of inorganic radicals in aqueous solution. J. Phys. Chem. Ref. Data 17, 1027–1284. http://dx.doi.org/10.1063/1.555808

Nithitanakool, S., Pithayanukul, P., Bourgeois, S., Fessi, H., Bavovada, R., 2013. The development, physicochemical characterisation and in vitro drug release studies of pectinate gel beads containing Thai mango seed kernel extract. Molecules 18, 6504–6520. http://dx.doi.org/10.3390/molecules18066504

Pan, X., Yan, L., Qu, R., Wang, Z., 2018. Degradation of the UV-filter benzophenone-3 in aqueous solution using persulfate activated by heat, metal ions and light. Chemosphere 196, 95–104. http://dx.doi.org/10.1016/j.chemosphere.2017.12.152

Pawar, S.N., Edgar, K.J., 2012. Alginate derivatization: A review of chemistry, properties and applications. Biomaterials 33, 3279–3305. http://dx.doi.org/10.1016/j.biomaterials.2012.01.007

Phang, S.W., Sin, L.T., Bee, S.T., Low, J.Y., Tee, T.T., 2018. Release behaviour study on controlled-release phosphorous fertilizer encapsulated by starch-alginate superabsorbent composite. J. Eng. Sci. Technol. 13, 82–94.

Phillips, G.O., Williams, P.A. (Eds.), 2000. Introduction to food hydrocolloids. In: Handbook of Hydrocolloids. Woodhead Publ Ltd, New York, pp. 1–19.

Pourjavadi, A., Farhadpour, B., Seidi, F., 2008. Synthesis and investigation of swelling behavior of grafted alginate/alumina superabsorbent composite. Starch/Staerke 60, 457–466. http://dx.doi.org/10.1002/star.200800208

Raju, K.M., Raju, M.P., 2001. Synthesis and Swelling Properties of Superabsorbent Copolymers 20, 146–154. http://dx.doi.org/10.1002/pi.721

Ranc, B., Faure, P., Croze, V., Lorgeoux, C., Simonnot, M.-O., 2017. Comparison of the effectiveness of soil heating prior or during in situ chemical oxidation (ISCO) of aged PAH-contaminated soils. Environ. Sci. Pollut. Res. 24, 11265–11278. http://dx.doi.org/10.1007/s11356-017-8731-0

Ranc, B., Faure, P., Croze, V., Simonnot, M.O., 2016. Selection of oxidant doses for in situ chemical oxidation of soils contaminated by polycyclic aromatic hydrocarbons (PAHs): A review. J. Hazard. Mater. 312, 280–297. http://dx.doi.org/10.1016/j.jhazmat.2016.03.068

Sahraei, R., Sekhavat Pour, Z., Ghaemy, M., 2017. Novel magnetic bio-sorbent hydrogel beads based on modified gum tragacanth/graphene oxide: Removal of heavy metals and dyes from water. J. Clean. Prod. 142, 2973–2984. http://dx.doi.org/10.1016/j.jclepro.2016.10.170

Santos, A., Fernandez, J., Rodriguez, S., Dominguez, C.M., Lominchar, M.A., Lorenzo, D., Romero, A., 2018. Abatement of chlorinated compounds in groundwater contaminated by HCH wastes using ISCO with alkali activated persulfate. Sci. Total Environ. 615, 1070–1077. http://dx.doi.org/10.1016/j.scitotenv.2017.09.224

Santos, A.F.M., Macedo, L.J.A., Chaves, M.H., Espinoza-Castañeda, M., Merkoçi, A., Limac, F.D.C.A., Cantanhêde, W., 2016. Hybrid self-assembled materials constituted by ferromagnetic nanoparticles and tannic acid: A theoretical and experimental investigation. J. Braz. Chem. Soc. 27, 727–734. http://dx.doi.org/10.5935/0103-5053.20150322

Satapanajaru, T., Chokejaroenrat, C., Sakulthaew, C., Yoo-iam, M., 2017. Remediation and restoration of petroleum hydrocarbon containing alcohol-contaminated soil by persulfate oxidation activated with soil minerals. Water Air Soil Pollut. 228, 345. http://dx.doi.org/10.1007/s11270-017-3527-x

Satapanajaru, T., Yoo-iam, M., Bongprom, P., Pengthamkeerati, P., 2015. Decolorization of reactive black 5 by persulfate oxidation activated by ferrous ion and its optimization. Desalin. Water Treat. 56, 121–135. http://dx.doi.org/10.1080/19443994.2014.932710

Sedlacek, O., Kucka, J., Monnery, B.D., Slouf, M., Vetrik, M., Hoogenboom, R., Hruby, M., 2017. The effect of ionizing radiation on biocompatible polymers: From sterilization to radiolysis and hydrogel formation. Polym. Degrad. Stab. 137, 1–10. http://dx.doi.org/10.1016/j.polymdegradstab.2017.01.005

Singh, K., Sinha, T.J.M., Srivastava, S., 2015. Functionalized nanocrystalline cellulose: Smart biosorbent for decontamination of arsenic. Int. J. Miner. Process. 139, 51–63. http://dx.doi.org/10.1016/j.minpro.2015.04.014

Sun, C., Dai, L., Gao, Y., 2017. Interaction and formation mechanism of binary complex between zein and propylene glycol alginate. Carbohydr. Polym. 157, 1638–1649. http://dx.doi.org/10.1016/j.carbpol.2016.11.046

Tsai, F.H., Kitamura, Y., Kokawa, M., 2017. Effect of gum arabic-modified alginate on physicochemical properties, release kinetics, and storage stability of liquid-core hydrogel beads. Carbohydr. Polym. 174, 1069–1077. http://dx.doi.org/10.1016/j.carbpol.2017.07.031

Wang, C., Liu, H., Sun, Z., 2012. Heterogeneous photo-fenton reaction catalyzed by nanosized iron oxides for water treatment. Int. J. Photoenergy 2012, 1–10. http://dx.doi.org/10.1155/2012/801694

Wang, W., Wang, A., 2010. Synthesis and swelling properties of pH-sensitive semi-IPN superabsorbent hydrogels based on sodium alginate-g-poly(sodium acrylate) and polyvinylpyrrolidone. Carbohydr. Polym. 80, 1028–1036. http://dx.doi.org/10.1016/j.carbpol.2010.01.020

Wang, W., Zhao, J., Zhou, N., Zhu, J., Zhang, W., Pan, X., Zhang, Z., Zhu, X., 2014. Reversible deactivation radical polymerization in the presence of zero-valent metals: From components to precise polymerization. Polym. Chem. 5 (11), 3533–3546. http://dx.doi.org/10.1039/c3py01398g

Wilske, B., Bai, M., Lindenstruth, B., Bach, M., Rezaie, Z., Frede, H.G., Breuer, L., 2014. Biodegradability of a polyacrylate superabsorbent in agricultural soil. Environ. Sci. Pollut. Res. 21, 9453–9460. http://dx.doi.org/10.1007/s11356-013-2103-1

Wu, F., Zhang, Y., Liu, L., Yao, J., 2012. Synthesis and characterization of a novel cellulose-g-poly(acrylic acid-co-acrylamide) superabsorbent composite based on flax yarn waste. Carbohydr. Polym. 87, 2519–2525. http://dx.doi.org/10.1016/j.carbpol.2011.11.028

Xu, L., Wang, J., 2012. Magnetic nanoscaled Fe_3O_4/CeO_2 composite as an efficient fenton-like heterogeneous catalyst for degradation of 4-chlorophenol. Environ. Sci. Technol. 46, 10145–10153. http://dx.doi.org/10.1021/es300303f

Yan, N., Li, M., Liu, Y., Liu, F., Brusseau, M.L., 2017. Kinetic and thermodynamic studies of chlorinated organic compound degradation by siderite-activated peroxide and persulfate. Water Air Soil Pollut. 228, 453. http://dx.doi.org/10.1007/s11270-017-3631-y

Yan, Q.-Z., Zhang, W.-F., Lu, G.-D., Su, X.-T., Ge, C.-C., 2005. Frontal copolymerization synthesis and property characterization of starch graft- poly(acrylic acid) hydrogels. Chem.-A Eur. J. 11, 6609–6615. http://dx.doi.org/10.1002/chem.200500554

Yang, Y., Pignatello, J.J., Ma, J., Mitch, W.A., 2014. Comparison of halide impacts on the efficiency of contaminant degradation by sulfate and hydroxyl radical-based advanced oxidation processes (AOPs). Environ. Sci. Technol. 48, 2344–2351. http://dx.doi.org/10.1021/es404118q

Yang, Z., Sheu, Y., Dong, C., Chen, C., Chen, S., 2020. Remediation of phenol-contaminated groundwater using in situ fenton and persulfate oxidation: performance and mechanism studies. Desalin. Water Treat. 175, 359–368. http://dx.doi.org/10.5004/dwt.2020.24827

Yong, T.J., Munusamy, Y., Chee, S.Y., 2015. The effect of acrylic acid and acrylamide graft-copolymerization on the properties of sodium alginate-based superabsorbent polymer. Int. J. Gen. Eng. Technol. 4, 1–14.

Yoo-iam, M., Satapanajaru, T., Chokejaroenrat, C., Sakulthaew, C., Comfort, S., 2020. Remediating phenol-contaminated groundwater and aquifer using persulfate oxidation. pp. 1–13. http://dx.doi.org/10.5004/dwt.2020.26439

Yu, C.L., Wang, X., Chen, C., Zhang, F., 2014. Preparation of polystyrene microspheres using rosin-acrylic acid diester as a cross-linking agent. Ind. Eng. Chem. Res. 53, 2244–2250. http://dx.doi.org/10.1021/ie402868y

Zhang, Y.Q., Xie, X.F., Huang, W.L., Huang, S., Bin, 2013. Degradation of aniline by Fe^{2+}-activated persulfate oxidation at ambient temperature. J. Cent. South Univ. 20, 1010–1014. http://dx.doi.org/10.1007/s11771-013-1577-9

Zhang, M., Zhang, S., Chen, Z., Wang, M., Cao, J., Wang, R., 2019. Preparation and characterization of superabsorbent polymers based on sawdust. Polymers 11 (1891), http://dx.doi.org/10.3390/polym11111891

Zhang, B.T., Zhang, Y., Teng, Y., Fan, M., 2015. Sulfate radical and its application in decontamination technologies. Crit. Rev. Environ. Sci. Technol. 45, 1756–1800. http://dx.doi.org/10.1080/10643389.2014.970681

Zhao, C., Zhong, S., Li, C., 2019. Property and mechanism of phenol degradation by biochar activated persulfate. Integr. Med. Res. 9, 601–609. http://dx.doi.org/10.1016/j.jmrt.2019.10.089

Zhao, C., Zhong, S., Li, C., Zhou, H., Zhang, S., 2020. Property and mechanism of phenol degradation by biochar activated persulfate. J. Mater. Res. Technol. 9, 601–609. http://dx.doi.org/10.1016/j.jmrt.2019.10.089